DEVELOPING SYNTHETIC MULTIVALENT CELLULAR EFFECTORS

A Dissertation
Presented to
The Academic Faculty

by

Chad Varner

In Partial Fulfillment
of the Requirements for the Degree
Doctor of Philosophy in the
School of Chemical and Biomolecular Engineering

Georgia Institute of Technology
August 2017

DEVELOPING SYNTHETIC MULTIVALENT CELLULAR EFFECTORS

Approved by:

Dr. Ravi Kane, Advisor
School of Chemical and Biomolecular Engineering
Georgia Institute of Technology

Dr. Krish Roy
School of Biomedical Engineering
Georgia Institute of Technology

Dr. Mark Prausnitz
School of Chemical and Biomolecular Engineering
Georgia Institute of Technology

Dr. M.G. Finn
School of Chemistry and Biochemistry
Georgia Institute of Technology

Dr. Hang Lu
School of Chemical and Biomolecular Engineering
Georgia Institute of Technology

Date Approved: July 13, 2017

To my family.

ACKNOWLEDGEMENTS

I would first like to acknowledge my advisor Ravi Kane, whose support has been vital through two universities. I would also like to thank the Faculty and Staff members of Rensselear Polytechnic Institute where I began my graduate studies. I would also like to thank the many friends there that I spent hours upon hours working with on homework. As our lab transitioned to Georgia Tech I received immeasurable support from the staff members here that enabled the transition to be as easy as possible. I would also like thank my committee members for their guidance and support. The other members of the Kane lab have been wonderful to work with and have made even the rough days enjoyable. Lastly, I would like to thank my wife, Missy, for letting me drag her across the country two times, and for being my support and release from lab work. Also, I would like to thank my children, Zina and August, for just being kids. Having a home to go to, even when chaotic, has made my work seem more meaningful and my days brighter and I wouldn't be here, or have learned what I learned, or have enjoyed the process without them and Missy. Thank you!

TABLE OF CONTENTS

ACKNOWLEDGEMENTS **iv**

LIST OF FIGURES **vii**

SUMMARY **ix**

CHAPTER 1. Introduction **1**
1.1 Multivalency in Biology Example: Influenza **1**
1.2 Engineered Multivalency: Targeting, Binding, and Inhibition **3**
1.3 Engineered Multivalency: Cellular Effectors **6**

CHAPTER 2. Directing the immune response to conserved epitopes on influenza hemagglutinin through antigen orientation **8**
2.1 Introduction **8**
2.2 Materials and Methods **12**
2.2.1 Generation of VLPs 12
2.2.2 Expression of HA 13
2.2.3 Adding streptavidin/HA to VLPS 13
2.2.4 Vaccine Characterization 14
2.2.5 Immunizations and Viral Challenge 14
2.3 Results **14**
2.3.1 Generation of VLP vaccines 14
2.3.2 Immunizations and viral challenges 19
2.4 Discussion **23**
2.5 Future work **25**

CHAPTER 3. Strain specific immunogenic responses to Respiratory Syncytial Virus Fusion Protein depend on Site Ø specificity **27**
3.1 Introduction **27**
3.2 Materials and methods **29**
3.2.1 Expression of Antibodies and RSVF 29
3.2.2 ELISA analysis 30
3.2.3 Vaccine construct assembly 30
3.2.4 Immunization 31
3.2.5 Serum analysis 31
3.3 Results **31**
3.3.1 Expression of RSVF and Glycan KO proteins 31
3.3.2 Expression of antibodies against RSVF 33
3.3.3 ELISA analysis of RSVF proteins 33
3.3.4 Expression and analysis of an RSVF B site Ø protein 33
3.3.1 RSVF vaccine design and assembly 37
3.3.2 Immunizations and Serum analysis 37
3.1 Discussion **41**

3.2 Future work 43

CHAPTER 4. Nanopatterning soluble protein antigens to guide immune recognition to desired epitopes 44
4.1 Introduction 44
4.2 Materials and methods 45
4.2.1 Protein expression and purification 45
4.2.2 PEGylation and purification 46
4.2.3 Purification of protein tagged GFP 47
4.2.4 Immunizations 47
4.2.5 Serum analysis 48
4.3 Results 48
4.3.1 Selecting PEG conjugation parameters 48
4.3.2 Expression, purification, and PEGylation of proteins 50
4.3.3 Elisa analysis of protein antigens 50
4.3.4 Immunization and serum analysis 56
4.1 Discussion 56
4.2 Future work 58

CHAPTER 5. Inducing cellular signaling through multivalency by controlling ligand display on polymer and polypeptide scaffolds 59
5.1 Introduction 59
5.2 Materials and methods 60
5.2.1 Generation of polypeptide scaffolds 60
5.2.2 Activating polypeptide scaffolds 60
5.2.3 Stem cell signalling tests 61
5.2.4 Antibody and Fab expression and purification 61
5.2.5 Wnt responsive luciferase reporter assay 61
5.3 Results 61
5.3.1 Expression and characterization of protein-based multivalent scaffolds 62
5.3.1 Activation with Ephrin-B4 peptide and stem cell differentiation. 62
5.3.2 Wnt Signaling assay 62
5.3.1 Antibody mediated signal inhibition 66
5.4 Discussion 66
5.1 Future work 70

CHAPTER 6. Conclusion 71

CHAPTER 7. Future Directions 72

REFERENCES 73

LIST OF FIGURES

Figure 1	Attachment of influenza virus to cell surface	2
Figure 2	B-cell activation upon multivalent binding of ligand	4
Figure 3	Examples of synthetic multivalent molecules	5
Figure 4	Multivalent molecules as cellular effectors	7
Figure 5	Structure of strain specific and broadly neutralizing antibodies to HA	9
Figure 6	Inverting HA orientation	11
Figure 7	Development of VLP-based influenza vaccines	15
Figure 8	Characterization of MS2 VLPs	17
Figure 9	Characterizing Streptavidin-VLPs	18
Figure 10	Expression of biotinylated HA	20
Figure 11	Characterization of HA coated vaccines	21
Figure 12	Vaccination and viral challenge after 3 injections	22
Figure 13	Chimeric H5/1N1 viral challenge after 2 injections	24
Figure 14	Crystal Structures of RSVF	28
Figure 15	Expression of RSV preF	32
Figure 16	RSVF antibody expressions	34
Figure 17	ELISA of RSVF proteins	35
Figure 18	Variability within Site 0	36
Figure 19	RSVF-B Site 0 mutations block Site 0 antibodies	38
Figure 20	RSVF vaccine design	39
Figure 21	Protein Gel of RSVF vaccine assembly	40
Figure 22	Serum depletion	42
Figure 23	Selecting mutants for site specific bioconjugation	49

Figure 24 Native-PAGE Separation of PEGylated GFP 51

Figure 25 SDS-PAGE of GFP antigens 52

Figure 26 MALDI-TOF spectra of non-PEGylated GFP antigens 53

Figure 27 MALDI-TOF spectra of PEGylated GFP antigens 54

Figure 28 GFP antigens selectively bind to antibodies 55

Figure 29 Wild Type and Spycatcher-GFP immunization results 57

Figure 30 Polypeptide scaffolds for multivalent display 63

Figure 31 Induced Ephrin-B4 signaling using polypeptide scaffolds 64

Figure 32 Expression and characterization of polypeptide scaffolds 65

Figure 33 Mechanism of Wnt signaling 67

Figure 34 Wnt signaling assay development 68

Figure 35 Anti-Fzd Ab inhibits Wnt signaling 69

SUMMARY

In my doctoral work, I have designed bioconjugates that can elicit desired cellular responses – cellular effectors. I have been particularly interested in using multivalent interactions, involving the simultaneous binding of multiple receptors to multiple ligands. In this dissertation, I have designed synthetic multivalent cellular effectors to use as vaccines and to direct stem cell fate. First, I have developed multivalent scaffolds to be used as a "universal" influenza vaccine based on virus-like particles (VLPs) displaying the influenza antigen hemagglutinin (HA). By site-specific bioconjugation, we have controlled the orientation of HA on the surface of the VLPs to make the conserved stalk region more accessible to the immune system. We have seen an enhanced stalk-directed immune response, and protection in mice against a challenge with influenza viruses presenting a chimeric hemagglutinin.

Using a similar strategy, we have developed vaccine constructs for Respiratory Syncytial Virus (RSV) that we are using to understand the importance and efficacy of a newly discovered antigenic site Ø (site Ø). We have already demonstrated the ability to tune the binding of anti-site-Ø antibodies to multivalent scaffolds presenting RSV antigens and immunization experiments with these scaffolds are currently underway. We have also developed a novel strategy for nanopatterning protein antigens to guide the immune response toward and away from desired epitopes. We have demonstrated the concept using green fluorescent protein (GFP) as a model antigen and are extending the concept to other antigens. This method could be broadly applicable to direct immune responses to conserved and highly efficacious epitopes on protein antigens.

I have also designed multivalent ligands that can modulate signaling pathways (e.g., Wnt and Eph signaling pathways). I have generated polypeptide-based scaffolds that can explicitly control the valency of multivalent conjugates as well as the inter-ligand spacing. In collaboration with UC Berkeley, we have shown that these polypeptide scaffolds can be used to induce stem cell signaling and that controlling the valency and spacing affects Eph-ephrin signal potentiation. We are also developing multivalent molecules comprised of antibody fragments bound to polymeric scaffolds to be effective at modulating Wnt signaling and that can potentially be used as therapeutics to modulate stem cell differentiation. Modulating the Wnt pathway has been difficult in the past due to the difficulty of expressing the Wnt ligand and the complexity of a dual-receptor-mediated signaling pathway. I have established the protocols that will be needed to validate the initial multivalent conjugates that will be made.

Using protein engineering tools, I have developed multivalent molecules that can direct cellular responses and have shown they are effective in stimulating immune and stem-cell signaling events. The scaffolds that I have developed can be used in other vaccine design and stem cell proliferation studies. The general application of nanopatterning protein antigens has already been applied to several other systems in our lab and we hypothesize that it will be broadly applicable in future antigen design studies. Thus, the work presented in this thesis will stand as a foundation for future studies in vaccine design and cell signaling studies.

CHAPTER 1. INTRODUCTION

Multivalent interactions – the simultaneous binding of several ligands on one moiety to several receptors on another – are ubiquitous throughout biology[1]. They range in size from protein-protein interactions at the nanometer scale to cell-cell interactions stretching over micrometers. The function of multivalency can vary from increasing affinity of ligands to targets to tuning response levels in signaling cascades or creating large contact surfaces between moieties[1]. For example, the affinity (or avidity) of a peptide ligand for a target protein can increased by over 5 orders of magnitude using multivalency[2,3]. The functions of multivalency are not mutually exclusive and biological and synthetic systems can benefit from the implementation of multiple modes of action. Thus, mimicking this natural phenomenon is a promising approach to developing novel therapeutics and bioactive molecules.

1.1 Multivalency in Biology Example: Influenza

A prime example of multivalent interactions in biology is the binding of a virus to a cell. Figure 1 depicts the binding of an influenza virus to a respiratory tract cell[4]. The hemagglutinin protein on the virus binds to sialic acid residues on the surface of cells. This interaction in its monovalent form has a millimolar dissociation constant (K_d)[5]. However, viral binding to sialic acid monomers shows a K_d ~ 10 μM[6], and binding the virus to synthetic molecules presenting sialic acid in a multivalent fashion (somewhat analogous to the surface of a cell) has reached a K_d ~ 600 pM[7,8].

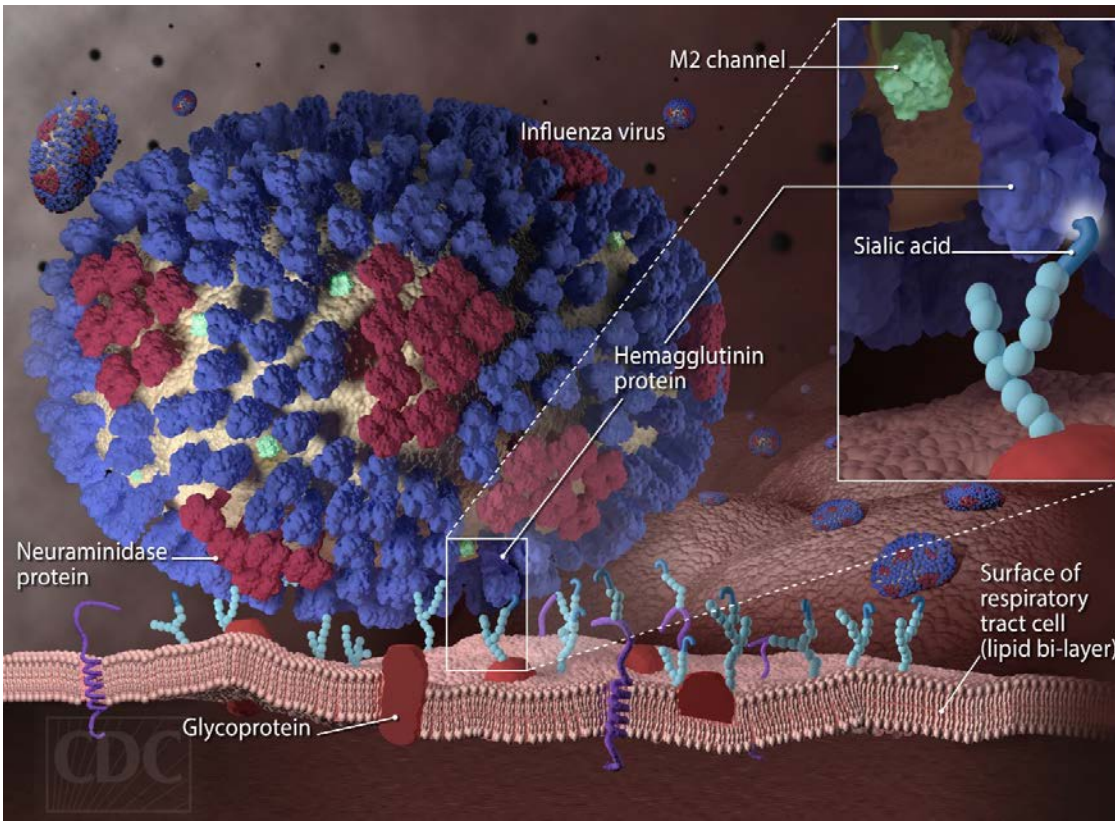

Figure 1. Attachment of influenza virus to cell surface. Viral attachment is mediated by the multivalent binding of hemagglutinin on the virus to sialic acid residues on the cell membrane. There are roughly 400 HA trimers on the viral envelope and several thousand sialic residues on cell surfaces. Image reprinted from http://www.cdc.gov/flu/images.htm

The multivalent nature of the virus also has ramifications for the immune response of the infected individual. B-cells, whether naive or memory related, carry antibodies on their surfaces as part of the B-cell receptor complex used to identify immunogens. Upon multivalent binding, the B-cell receptors are clustered together and induce a signaling cascade within the cells (Figure 2) that triggers a larger immune response[9]. Thus, not only does multivalent binding enhance the binding of B-cells to their immunogens but there is an overall activation of the cell in response.

1.2 Engineered Multivalency: Targeting, Binding, and Inhibition

As shown with influenza, multivalent interactions can increase the affinity of a ligand for its target dramatically. Thus, synthetic multivalent molecules are well poised to be used for targeting and adhesion. Further, pathogen inhibitors can be improved by mimicking and disrupting the multivalent interactions that pathogens use to bind to their hosts. Several reviews highlight how nanoparticle- and polymer-based multivalent displays find therapeutic usage[1,10–18]. Figure 3 highlights a few recent papers that demonstrate how the enhanced binding of multivalent systems can be beneficial for therapeutics.

In Figure 3A, Rhee et al. were able to target cells expressing the CD22 receptor by covalently attaching a glycan to the surface of a virus-like particle (VLP)[19]. While unconjugated VLPs did not bind to cells, the glycan coated VLPs selectively bound to target cells and were able to be used as photodynamic killing agents. In Figure 3B, Kang et al. developed a modular platform that can display any antibody of choice on a multivalent ferritin nanoparticle[20]. The antibodies are bound to the nanoparticle non-covalently via an

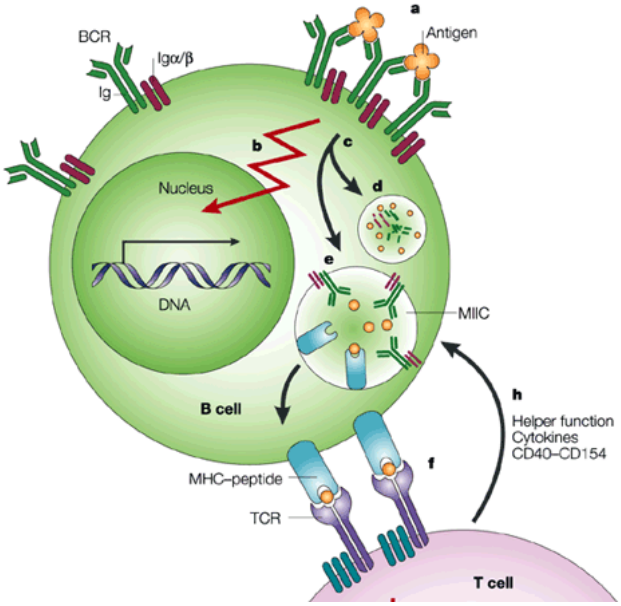

Figure 2. B-cell activation upon multivalent binding of ligand. The antibodies on the surface of B-cells cluster together upon ligand binding. The clustering of the intracellular domain of the B-cell receptor complex induces the overall activation of the cell. Reprinted from Pierce, 2002, with permission[9].

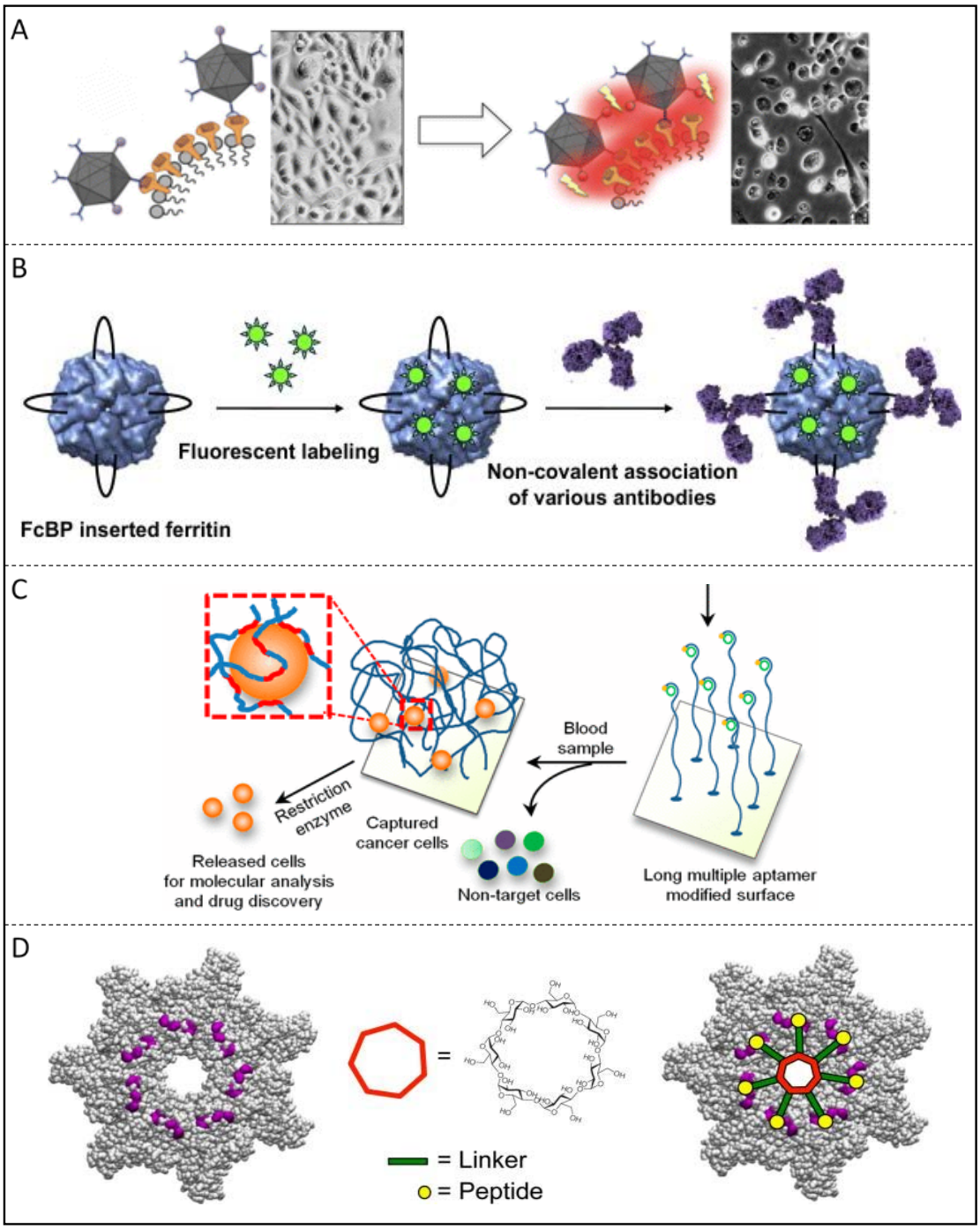

Figure 4. Examples of synthetic multivalent molecules for targeting, binding and inhibition. (A) Glycan directed targeting of VLPs for photodynamic killing (Rhee, 2012)[19]. (B) Nanoparticle-based multivalent display of targeting antibodies (Kang, 2012)[20]. (C) Multivalent DNA aptamer hydrogel for capturing cancer cells (Zhao, 2012)[21]. (D) β-cyclodextrin-based inhibitor of anthrax toxin (Joshi, 2011)[2]. All figures reprinted with permission.

Fc-binding peptide. These nanoparticles were subsequently targeted to HER2 expressing cancer cells as a proof of principle.

Multivalent polymers have also been used to enhance avidity of binding ligands. Figure 3C shows how Zhao et al. created multivalent networks of protein tyrosine kinase 7 (PTK7)-binding aptamers based on the biopolymer DNA[21]. PTK7 is overexpressed on certain leukemia cells and served as a multivalent handle to pull down cancer cells from whole blood. Joshi et al. used β-cyclodextrin to develop anthrax toxin inhibitors (Figure 3D)[2]. The multivalent display of the peptide ligand decreased the half-maximal inhibitory concentration (IC_{50}) of the inhibitor by over five orders of magnitude.

1.3 Engineered Multivalency: Cellular Effectors

Another niche that multivalent molecules fill is that of cellular effectors. As exemplified in B-cell-antigen interactions (Figure 2), many cellular processes are controlled by the clustering of membrane bound receptors[1,22–24]. Again, this natural phenomenon has been copied by researchers to both study and artificially modulate various signaling cascades including those involved in immune responses[25–30] and cellular differentiation and growth[31–35]. Webber et al. designed a vascular endothelial growth factor-based peptide amphiphile (VEGF-PA) that assembled into nanofiber gel networks (Figure 4A)[35]. In an in vivo chicken chorioallantoic membrane (CAM) assay the VEGF-PA showed markedly enhanced blood vessel generation compared to the peptide alone; the multivalent display of the VEGF peptide increased angiogenesis by almost 4-fold. In another study, Conway et al. conjugated ephrin-B2 to hyaluronic acid to cluster Eph receptors and induce neural stem cell differentiation into dopaminergic neurons (Figure 4B)[31]. They saw that the multivalent ephrin-B2 promoted differentiation better than monovalent and Fc-conjugated

bivalent ephrin-B2. Conway also found that the density of ephrin-B2 proteins conjugated to the linear polymer backbone correlated with downstream signaling strength.

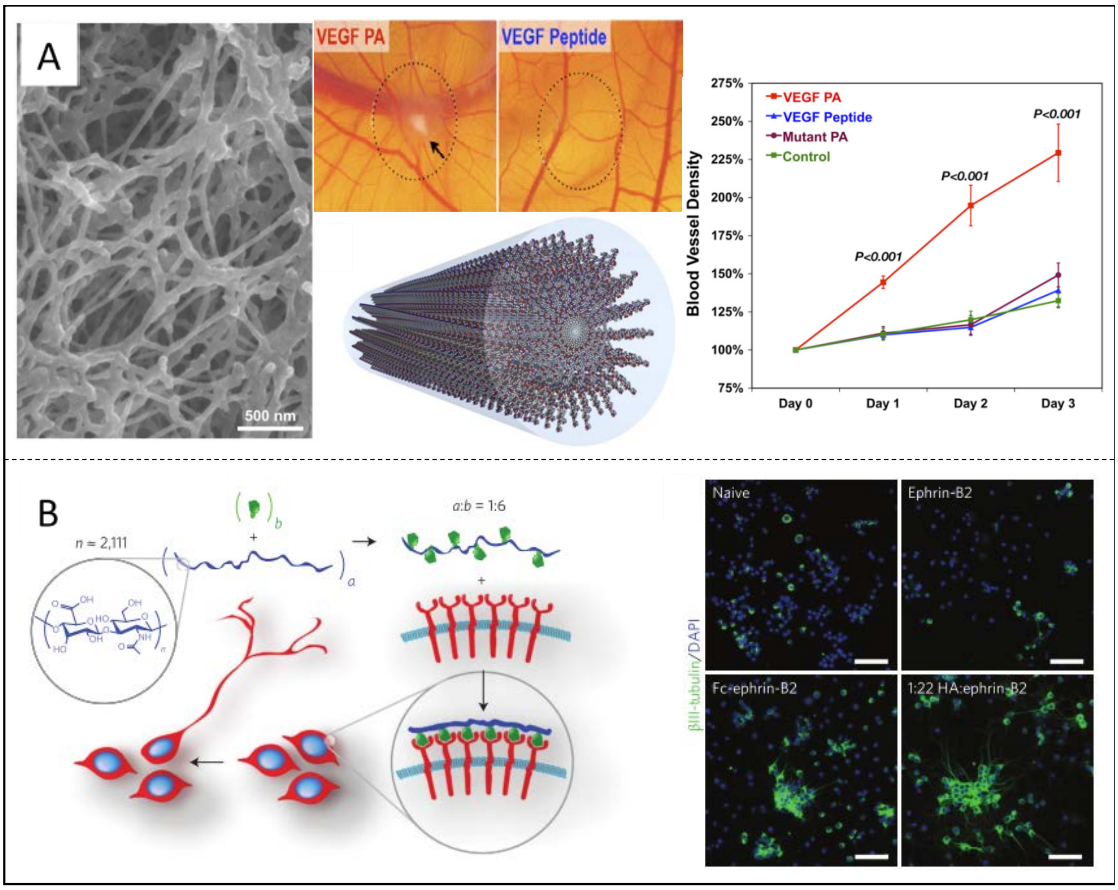

Figure 4. Multivalent molecules as cellular effectors. (A) VEGF-peptide amphiphiles (VEGF-PA) were designed to assemble into nanotubes and formed network hydrogels (Webber, 2011)[35]. Blood vessel density correlated to angiogenesis in an in vivo CAM assay. (B) Ephrin-B2 was conjugated to hyaluronic acid polymers and induced receptor clustering (Conway, 2013)[31]. Differentiation of rat neural stem cells was visualized by immunostaining cell specific markers. in vitro and in vivo. Figures adapted and printed with permission.

CHAPTER 2. DIRECTING THE IMMUNE RESPONSE TO CONSERVED EPITOPES ON INFLUENZA HEMAGGLUTININ THROUGH ANTIGEN ORIENTATION

2.1 Introduction

It is estimated that influenza epidemics cause 250000-500000 deaths worldwide each year[36]. The global health challenge influenza viruses present is due in part to their ability to rapidly mutate to evade the immune system. Moreover, influenza vaccines elicit antibody responses directed primarily to the globular head domain on the hemagglutinin protein (HA)[37–39]. This immunodominant epitope on HA varies widely from strain to strain and across subtypes of influenza, thus necessitating seasonal Influenza vaccines[40]. HA does have exposed conserved domains, but the high immunogenicity of the globular head region that protrudes away from the virus leads to very few antibodies being raised against the conserved stalk domain[41].

Figure 5 shows several antibodies binding to HA[42]. Four of these, HC19, HC45, HC63, and HC151, bind to the head region and are strain specific. However, CR6261, which binds to the stalk of HA, is broadly neutralizing. Similarly, stalk-specific antibodies isolated from human sera show broad neutralization activity[43–45]. The stalk of HA, which is needed for membrane fusion after the virus has adhered to the cell, is highly conserved across various subtypes of Influenza. Thus, this epitope is less likely to undergo antigenic drift unlike the nonessential head domain. These facts suggest that if we can target the immune response to the stalk region of HA instead of the head domain, then we could elicit broadly neutralizing antibodies against influenza that could be active from year to year and end the need to receive seasonal flu vaccines. Indeed, because stalk-specific antibodies can neutralize influenza infections both by prophylaxis and by direct therapeutic

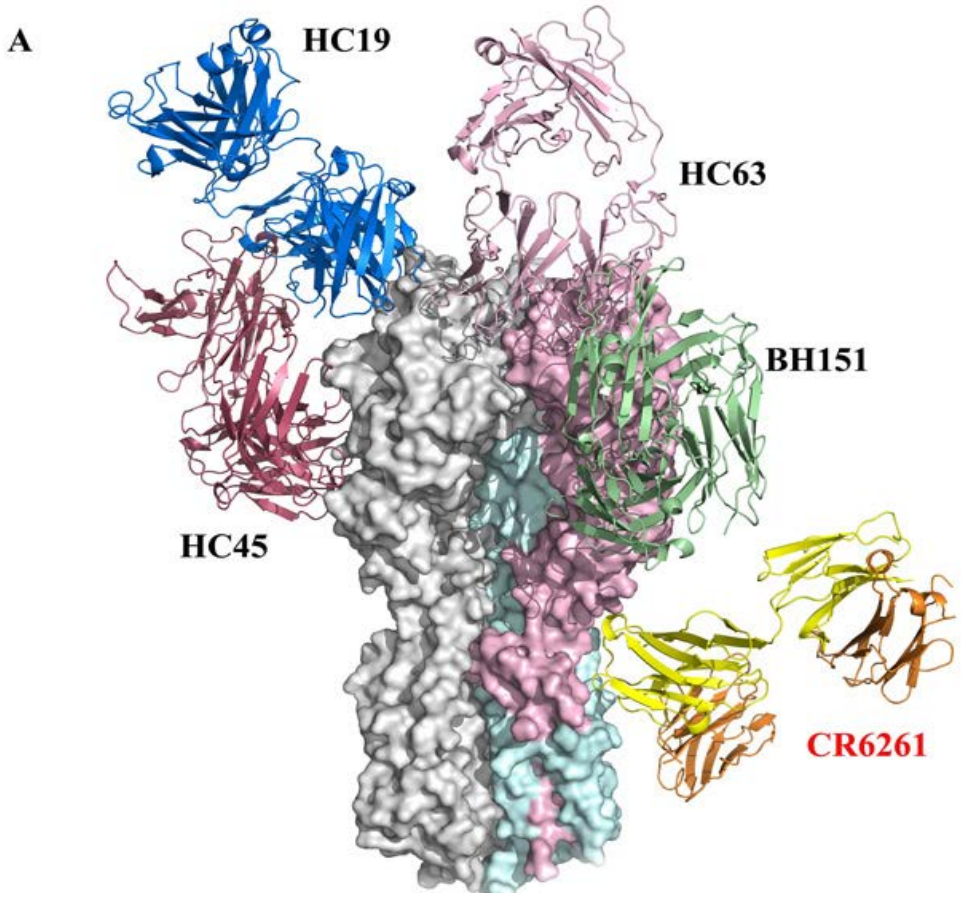

Figure 5. Structure of strain specific and broadly neutralizing antibodies to HA[42]. HA (surface structure) binds to several strain specific antibodies at its globular head domain. CR6261, however, binds to the highly conserved stalk region and is thus broadly neutralizing. Reprinted with permission from Ekiert, 2009[42].

administrations[42,4643,44,47,48] have led many researchers to try and develop vaccines that induce stalk specific immune responses.

One effort to generate stalk specific immune responses is by using chimeric HA proteins[46,49]. In brief, the stalk domain of HAs that are of concern for seasonal epidemics or pandemics are fused to the head domains of rare HAs that our immune systems are naïve to. Sequential immunizations with repeated HA stalks and changing HA heads lead to affinity maturation of antibodies specific to the stalk domain of HA. This vaccination approach yield antibodies that are effective against heterosubtypic viral challenges (i.e., antibodies generated against H1 are effective against H5 viruses). However, the display of these chimeric HAs in terms of traditional vaccines (rosettes on a virion) could lead to lower stalk-directed response than desirable.

In an effort to display HA with greater accessibility to the stalk domain, Kanekiyo et al fused HA to ferritin, which self assembles into nanoparticles[50]. The geometry of the ferritin particle makes the stalk of HA more accessible; causatively, these nanoparticle-based vaccines elicited antibodies that could neutralize several influenza strains within the same subtype.

In order to remove all head specific antibodies, recent reports have shown the ability to stabilize the stalk of HA in absence of the head domain[51–58]. Implagliazzo et al.[51] and Yassine et al.[52] both recently and independently reported stabilized headless- HAs that elicited stalk reactive antibodies active against influenza of different subtypes. Potential drawbacks of this approach include that by cutting off the head domain regions of the stalk that are blocked during infection are now available for antibody binding, and that generating these headless HAs has been extremely difficult and the fact that it has worked for one subtype does not mean that it will be feasible with different subtypes and groups of HA.

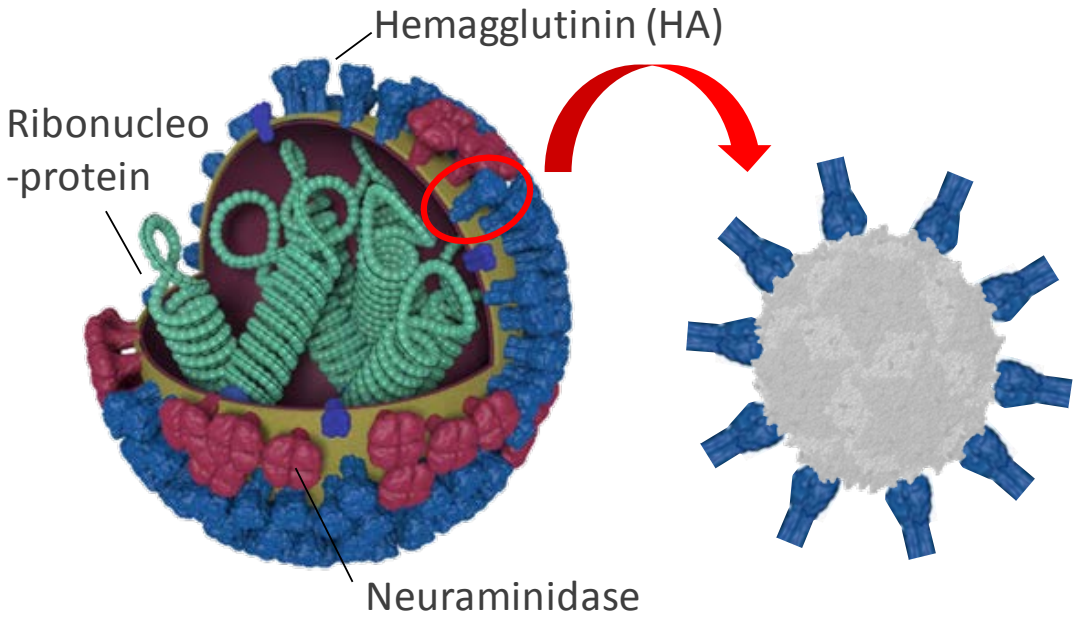

Figure 6. Inverting HA orientation. The HA ectodomain will be attached to a nanoparticle (virus-like particle) in the inverse orientation from that of the native virus. The inverted orientation should lead to more stem directed antibodies being generated. Adapted with permission from the CDC[4].

We hypothesized that by reversing the orientation of HA on the surface of a vaccine (illustrated in Figure 6[4]) we can increase the relative immunogenicity of the stalk region and elicit broadly neutralizing antibodies. In this way, we will keep the native sequence of the virus, and the only antigen that is presented to the immune system is the antigen of choice. Our method for displaying HA in this way is based on virus-like particles (VLPs). VLPs have been targeted for vaccine development by many researchers [59–61]. We have used the bacteriophage MS2 to display Hemagglutinin in both native and inverse orientations and have seen directly that reversing the orientation of HA generates a more protective immune response.

2.2 Materials and Methods

2.2.1 Generation of VLPs

MS2 VLPs were chosen as a scaffold because they have been shown to tolerate short insertions in the AB loop of the coat protein[62]. We generated a single chain dimer of MS2 with the avitag (GLNDIFEAQKIEWHE) inserted into the AB loop at residue 13 of the second monomer in the dimer chain. The coding DNA was E coli optimized and synthesized by Genscript and cloned into the pet28b between Nde1 and XhoI. pET28b-MS2AviDimer and pAcm-BirA (Avidity, LLC) were co-transformed into BL21(DE3) and grown in 2xYT media with 50 µg/ml kanamycin and 25 µg/ml chloramphenicol. 5 ml overnight cultures were added to 1 L 2xYT media. To induce expression and in vivo biotinylation, 1 mM IPTG and 50 µM D-biotin were added at OD=0.5-0.8 and cells were allowed to grow overnight at 30ºC. Cells were lysed by sonication and VLPs were purified on the GE Capto Core 700 resin. Purified MS2AviDimer was confirmed by gel

electrophoresis and biotinylation was confirmed by western blot, and VLP assembly was confirmed by dynamic light scattering and size exclusion chromatography.

2.2.2 Expression of HA

Influenza hemagglutinin was expressed and purified as previously described[63]. Insect optimized DNA was synthesized and cloned into pFastBac-Dual by General Biosystems under the p10 promoter. Insect optimized DNA coding for the biotin ligase BirA was cloned into the HA containing vectors under the polyhedron promoter to allow for in vivo biotinylation. Plasmids received were then transformed into DH10Bac competent cells as per manufacturer protocol. DNA was isolated via the PureLink miniprep protocol and used to generate baculovirus as described. Protein expression was carried out in Hi5 cells and proteins were purified by IMAC followed by SEC.

2.2.3 Adding streptavidin/HA to VLPS

Vaccine assembly was done in a two-step process. First, MS2 VLPs were added dropwise to 10-fold molar excess of 1 mg/ml streptavidin (Rockland) relative to avitag sites. After stirring for 1 hr at room temperature, the mixture was loaded onto a stepwise sucrose gradient (equal volumes 4%, 10%, and 30% sucrose in PBS) and spun at 31,000 rpm for 16-18 hrs in a SW-32Ti rotor. The top 29mL of the gradient were discarded and the pelleted streptavidin-coated VLPs were resuspended followed by desalting through a PD10 column. Then, HA was added to the streptavidin VLPs in a 2:1 molar ratio to streptavidin and incubated with stirring for 1 hr at room temperature. The assembled vaccines were purified again by sucrose gradient and the loading of HA onto the final vaccine constructs was verified by western blot.

2.2.4 Vaccine Characterization

Vaccines were characterized by several methods. SDS-PAGE and western blots were used to confirm the purity and presence of the vaccine subunit proteins. Transmission electron microscopy was performed by coating proteins on formvar treated Cu grids and negative staining with uranyl formate. For gold labeling, streptavidin VLPs were mixed with biotin-gold nanoparticles and then coated and stained. Images were collected on a Hitachi HT7700. Dynamic Light Scattering was performed on a Wyatt Dynastar reader.

2.2.5 Immunizations and Viral Challenge

Immunizations with vaccines were carried out by Florian Krammer at the Mount Sinai School of Medicine. In short, poly I:C was added to the VLP samples immediately prior to injection. 5 µg of HA were injected per mouse intramuscularly in a volume of 55 µl. The vaccinations happened every 21 days. All vaccines were tested with n=5 female BALB/C mice 6-8 weeks old. Viral challenges were performed by challenging the mice with 2.5 LD_{50} of an cH5/1N1 influenza virus. Weights were tracked and mice were euthanized when body weight dropped below 75% of initial. All animal experiments were performed in accordance with MSSM standard ethics protocols.

2.3 Results

2.3.1 Generation of VLP vaccines

We have developed a vaccine platform based on virus-like particles (VLPs) made from the bacteriophage MS2. Figure 7 outlines our approach to use MS2 VLPs as vaccine scaffolds. First, a single biotinylation site was introduced into a single-chain dimer of the

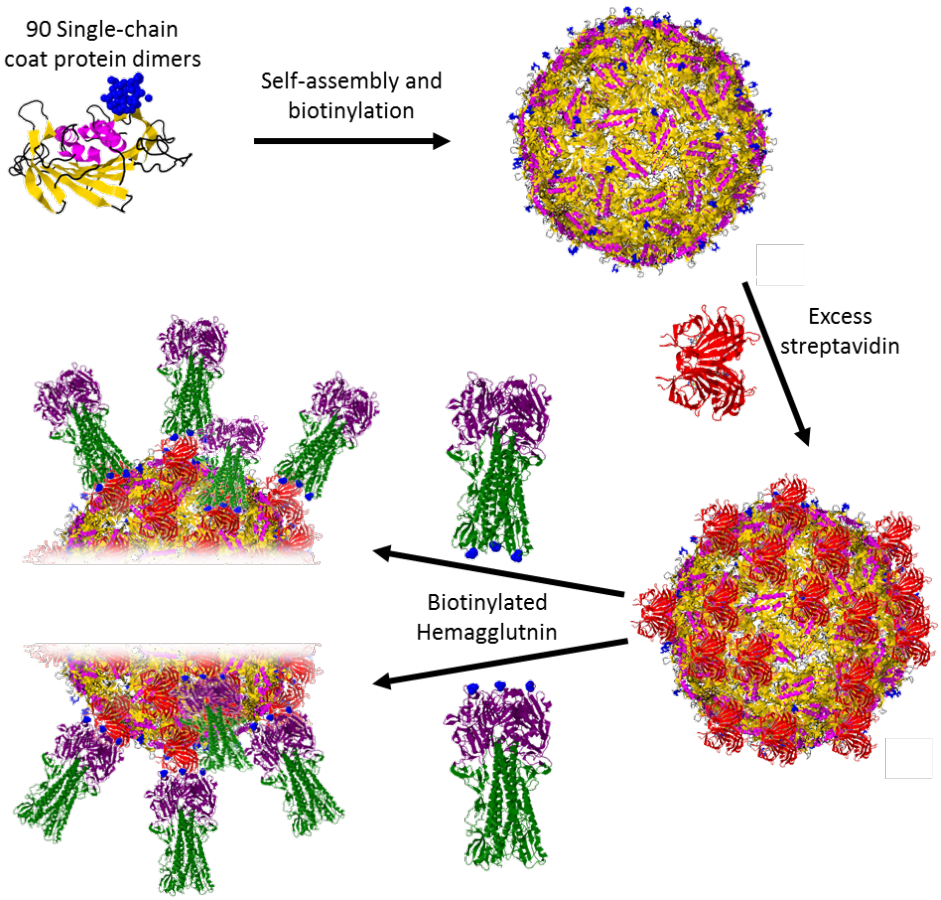

Figure 7. Development of VLP-based influenza vaccines. Single-chain MS2 coat protein dimers self-assemble into 27nm VLPs with 90 dimers. The biotin VLPs are bound to streptavidin and result in a streptavidin coated nanoparticle. Finally, HA biotinylated at either the tail end (native display, top) or head domain (reverse display of HA, bottom) is bound to make vaccines. Images including assembled VLPs are to scale. PDB IDs: 1MSC, 1STP, 2MS2, and 1RU7.

MS2 coat protein at the AB loop[62]. These proteins are both biotinylated and assembled into VLPs in vivo by co-expression with a Biotin ligase enzyme. Once self-assembled, 90 dimers form a roughly 27 nm particle with icosahedral symmetry[64]. The purity and assembly of the VLPs were verified by SDS-PAGE, DLS and TEM (Figure 8). VLPs were coated on transmission electron microscopy (TEM) grids and negatively stained. The particles show a diameter of roughly 30 nm which is consistent with the 27 nm diameter reported (Figure 8)[64].

The VLPs were then coated with excess streptavidin. Streptavidin is tetravalent in binding biotin, with a K_d of close to 10^{-14} M; it is one of the strongest non-covalent bonds known[65]. The biotin binding sites are available on opposite sides of streptavidin, and after quenching the surfaces of the VLPs, the particles become reactive to biotin again. Streptavidin coated VLPs were purified from free protein by ultracentrifugation through a sucrose cushion. The coating was confirmed to have equal mass of streptavidin and MS2 protein by SDS-PAGE and densitometry, which corresponds to the surface of the particles being completely covered. Furthermore, DLS confirmed an increase in the average particle diameter and TEM revealed that biotinylated gold particles bound to the surface of the streptavidin coated VLP (Figure 9). We have concluded that this behavior was biotin-mediated because when particles were quenched with excess biotin no attachment was seen (data not shown).

The activated scaffold was then ready to be coated with biotinylated HA antigen. We expressed and purified HA as previously described[63]. An Avitag sequence was incorporated either in the head domain or at the tail end of HA to allow for site-specific biotinylation. To confirm the proper folding and trimeric assembly of HA, I ran purified

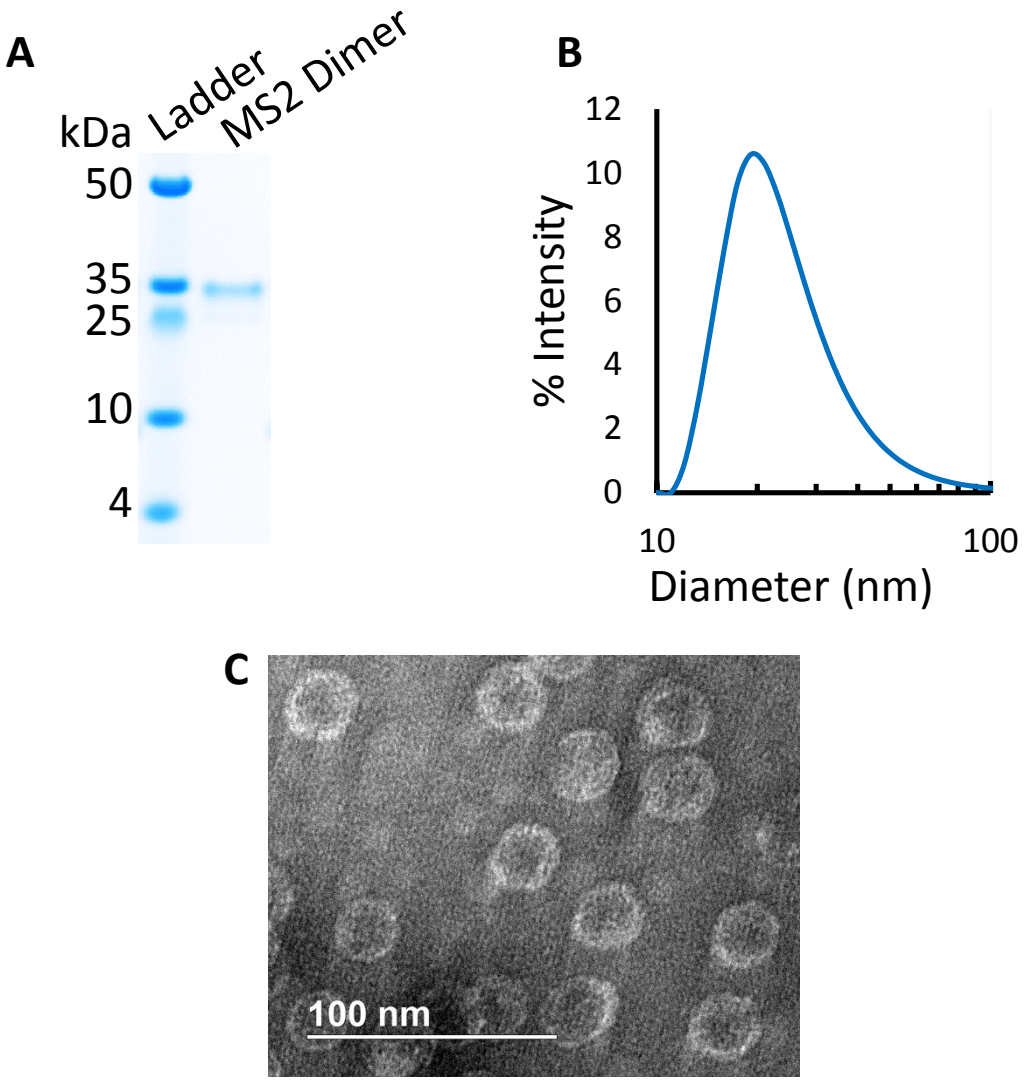

Figure 8. Characterization of MS2 VLPs. (A) Purified protein was run on SDS-PAGE to verify purity. (B) Size measurements were made with dynamic light scattering. (C) VLPs were imaged after negative staining in TEM, showing an average diameter of ~27nm.

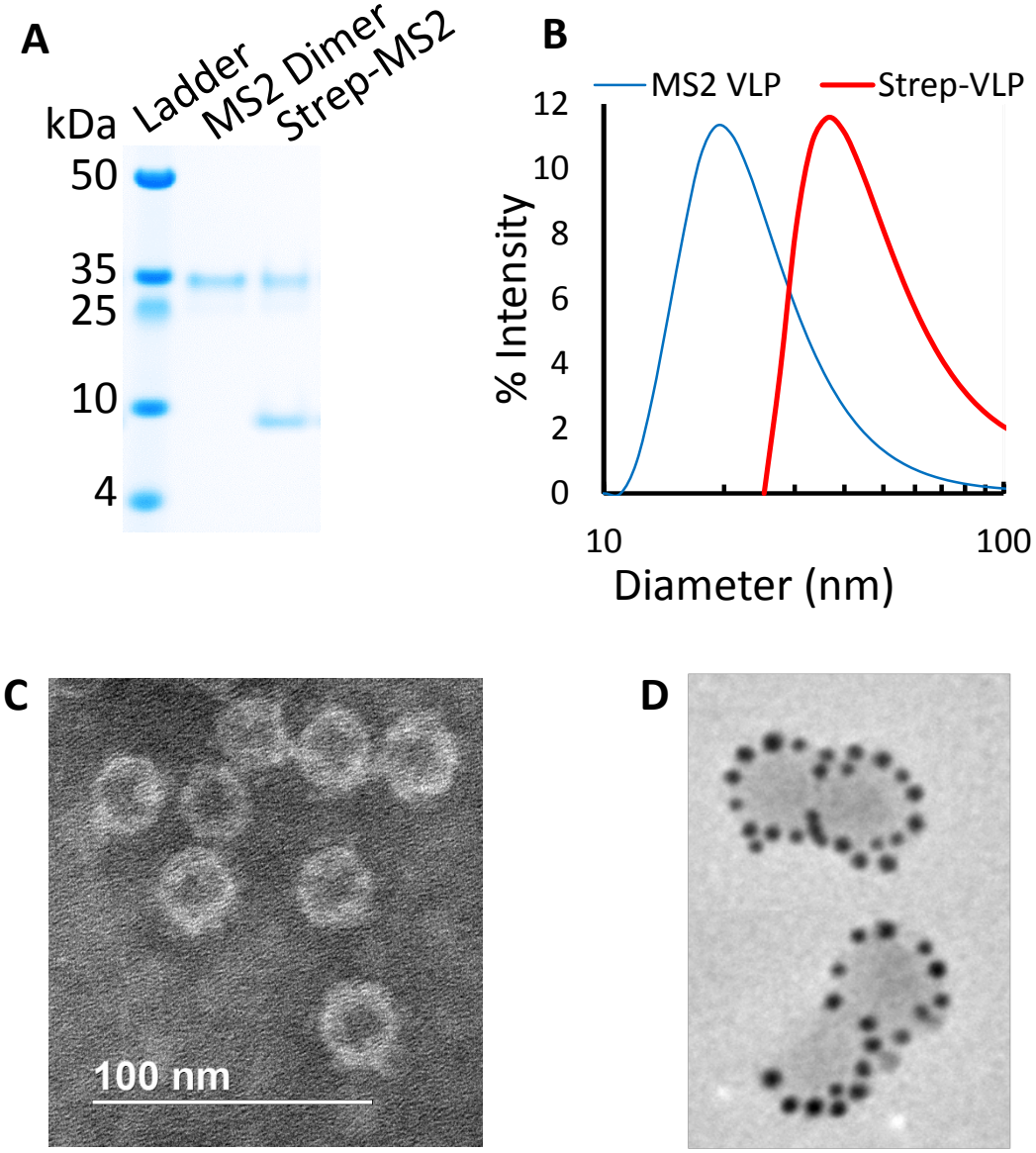

Figure 9. Characterizing Streptavidin-VLPs. (A) Commassie stained SDS-PAGE reveals that streptavidin is bound to the MS2 particles. (B) DLS shows an increase in average diameter of the particles. (C) TEM after negative staining shows particles retain structure and have a protein coat on their surface. (D) Particles were mixed with biotin-labeled gold nanoparticles and coated on a TEM grid.

HA through SEC-MALS. We were able to express and purify HA to homogeneity and confirmed that we did assemble trimeric protein (see Figure 10). ELISA analysis further revealed that both biotinylated versions of HA bound to a conformationally specific antibody, thus also verifying proper folding.

Coating the activated VLPs with either version of biotinylated HA trimer resulted in two testable vaccines, one presenting HA in the reverse orientation (head biotinylated), and one presenting HA in the native conformation, similar to the natural virus (HA biotinylated at the stem). VLP-HA conjugates were also analyzed by TEM (Figure 11). While exact characterization of the HA on the surface is difficult, the particles do appear to have a thicker protein shell than VLPs alone and there are proteins protruding from the surface. Based on quantification tests by BCA assays and semi-quantitative western blots, we generally achieved 10 HA trimers per VLP. This corresponds to about 350 nm^2 per HA trimer on the VLP surface compared to roughly 60 nm^2 per HA trimer on the viral envelope[66]; thus, HA on the VLP scaffolds is much less densely packed than on the virus.

2.3.2 Immunizations and viral challenges

We then sought to test if these VLP vaccines could induce the production of broadly neutralizing antibodies. In the labs of our collaborators at the Mt. Sinai School of Medicine, the first vaccination course performed used three vaccinations carrying an H1 subtype of HA. A viral challenge was performed using a chimeric HA with the stalk of H1 but the head domain of H5 (Figure 12). This challenge probed for antibodies that were generated against the stalk of HA specifically. Mice were protected from the chimeric H5/1 virus regardless of HA orientation – suggesting the stalk of HA was available to elicit an

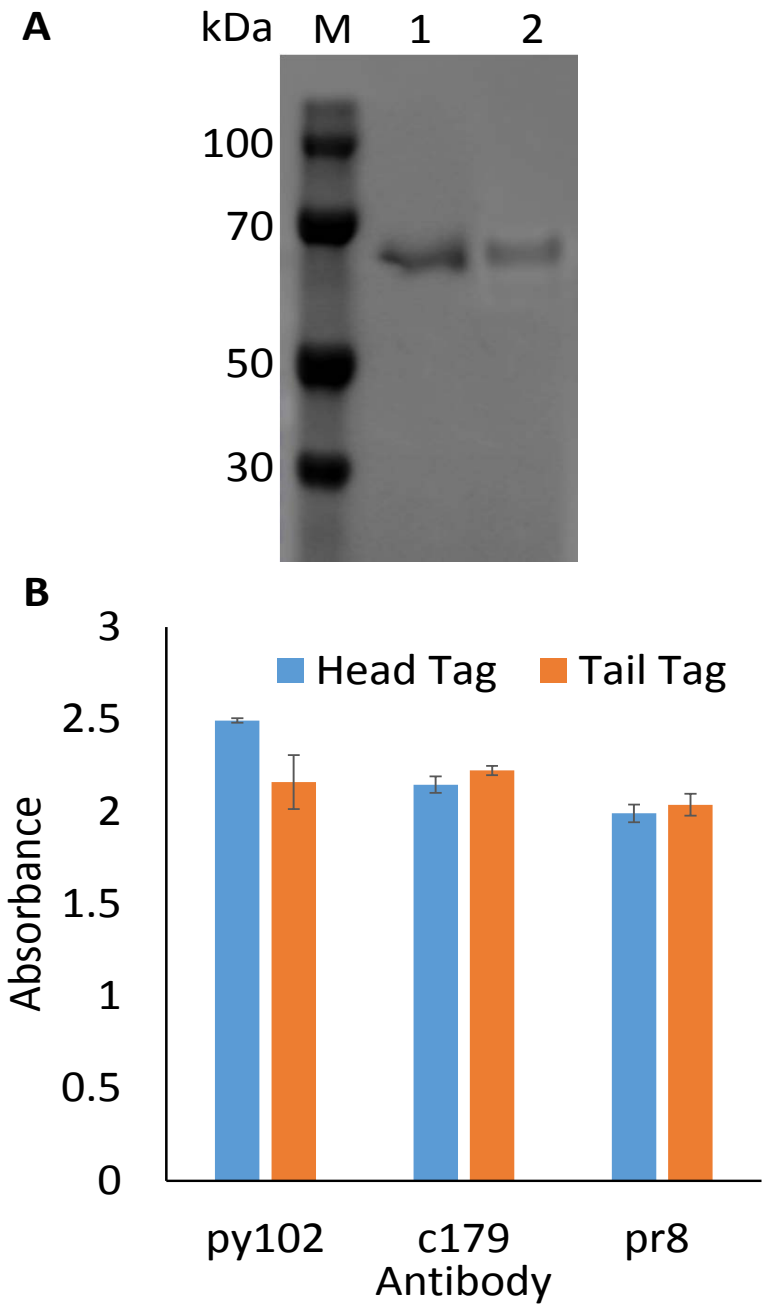

Figure 10. Expression of biotinylated HA. (A) SDS-PAGE of biotinylated HA after purification. Lanes: M-marker, 1- Head-biotinylated HA, 2 – tail biotinylated HA. (B) ELISA of expressed HA with three anti-HA antibodies, py102 and pr8 bind to the head domain of HA and are non-conformational, while c179 binds to the stalk of HA and is a conformational antibody.

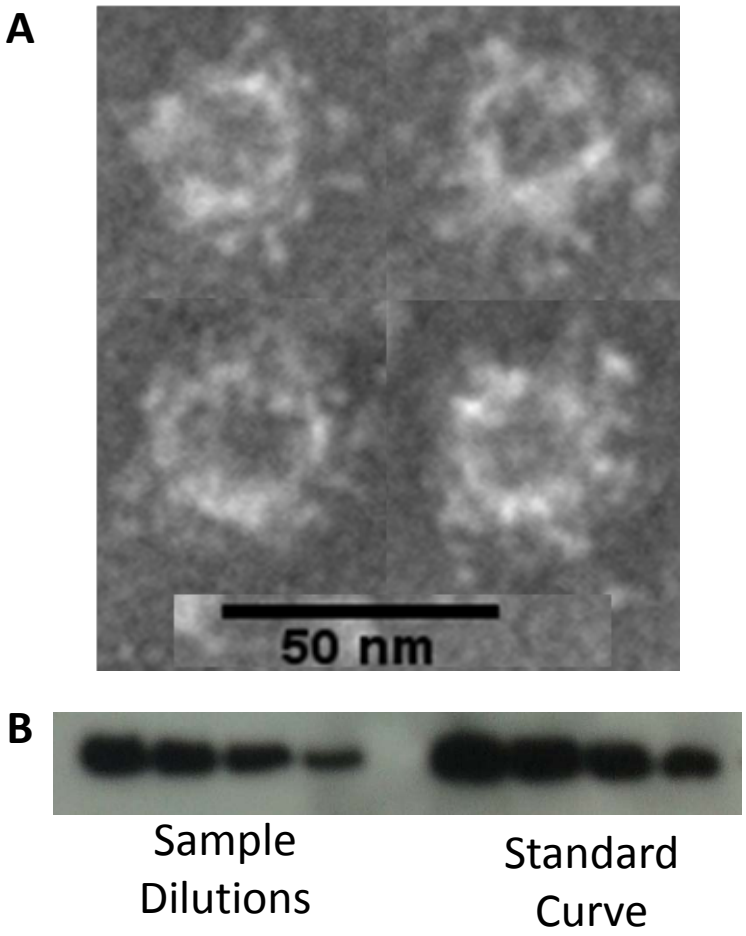

Figure 11. Characterization of HA coated vaccines. (A) TEM of full vaccine particles reveal a large protein coat, consistent with HA attachement. (B) A representative western blot used to detect and quantify the amount of HA in the vaccine constructs.

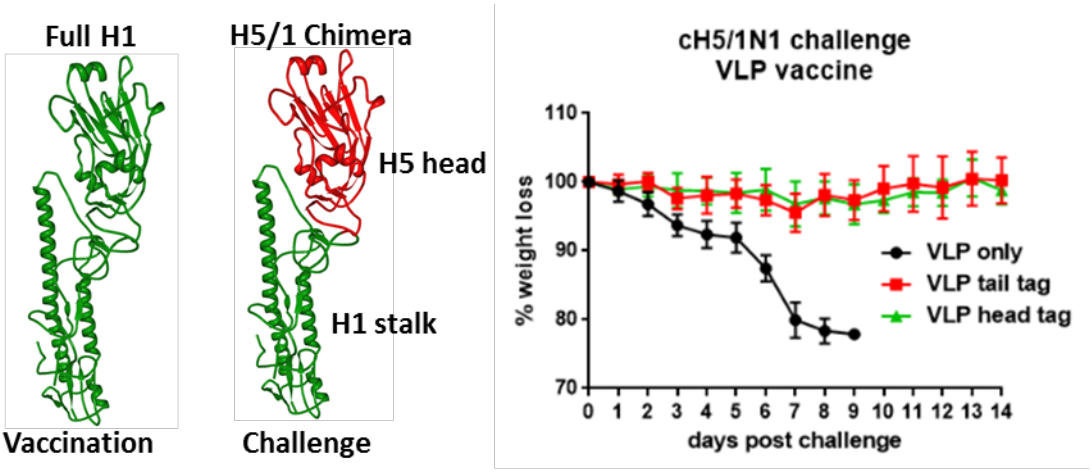

Figure 12. Vaccination and viral challenge after 3 injections. Full length H1 was used as the immunogen on VLPs in three injections. A chimeric H5/1 virus having an H5 head and H1 stalk was used to challenge. Data points on the right are the average of 5 mice. Tail tag refers to native presentation of HA, Head tag the inverted presentation of HA.

immune response whether it was proximal or distal to the surface of the VLP. This is not surprising as a recent influenza vaccine based on ferritin particles saw a similar response[20]. We hypothesize that because the HA particles are about 5- to 6-fold less packed on the VLP as they are on the virus they are more accessible to the immune system than when presented from the surface of the influenza virus. Serology tests suggested that there was a slight difference in the generation of stalk-specific antibodies after two injections that was then lost after the third injection.

This encouraged us to proceed with another round of vaccinations, this time only with two injections (Figure 13). The difference in protection was clear after two immunizations. Mice immunized with HA in the reverse orientation were fully protected while only 60% of the group immunized with HA in the native conformation survived. Thus, the generation of anti-stalk antibodies appears be promoted better by orienting the stalk outward than when the stalk is partially covered by the head domain.

2.4 Discussion

We have developed VLP-based scaffolds that can be used to display any biotinylated protein. By site-specifically biotinylating proteins by inserting the epitope recognized by the Biotin ligase enzyme BirA, antigenic proteins can be loaded onto the scaffold in a defined orientation. This streptavidin coated particle is similar to other plug and play scaffolds that allow for any antigen of choice to be loaded[67]. VLP scaffolds do have the potential challenge associated with generating antibodies against the scaffold itself rather than against the exposed antigen, which has been discussed in previous reports[59,61,68]. Still,

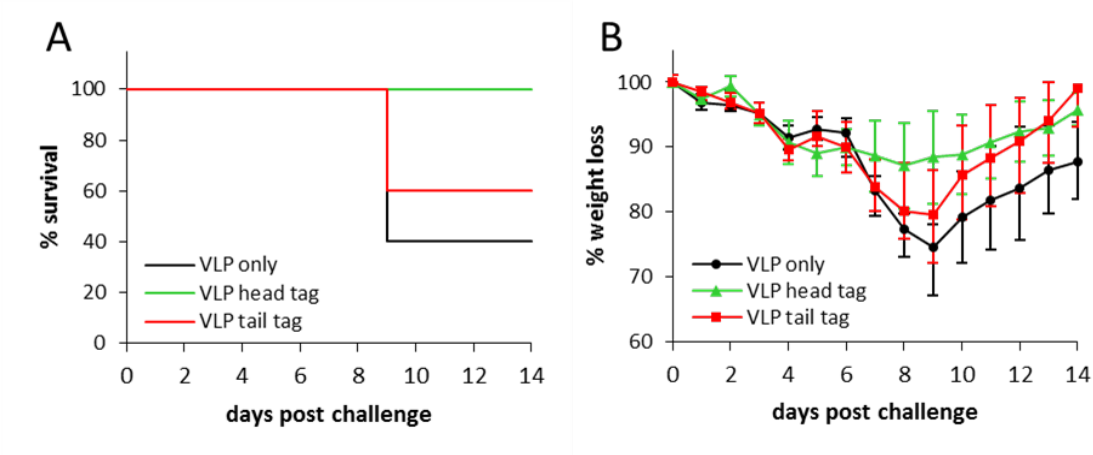

Figure 13. Chimeric H5/1N1 viral challenge after 2 injections. (A) Percent survival of the 5 mice in each group challenged. Tail tag refers to native presentation of HA, Head tag the inverted presentation of HA. (B) The average weight of living mice was normalized for initial weight and plotted for each vaccine construct.

these scaffolds are well suited to generating strong immune responses even in the absence of adjuvant[59,67,69,70].

We have used this multivalent streptavidin scaffold to display an H1 subtype HA from influenza in both the native orientation which leads the globular, immunodominant head to be highly exposed and in the inverse orientation resulting in the highly-conserved stalk to be exposed. Controlling the orientation altered the ability of our vaccines to induce protective levels of stalk-specific antibodies. These results suggest that the accessibility of the HA stalk is a factor in the limited generation of stalk-specific antibodies via traditional vaccines or natural infection. Furthermore, simply by controlling the orientation of HA to a nanoscale scaffold, we have redirected the immune response to the conserved stalk epitope, thus showing the potential of this scaffold to be used as a universal influenza vaccine that would elicit broadly active antibodies across several strains of influenza.

2.5 Future work

The initial viral challenge data looks very promising. Similar vaccinations will be performed using scaffolds functionalized with HA (purified by both affinity chromatography and SEC) and will be followed by a fully heterologous viral challenge with an H5/N1 virus. Additionally, the serum will be analyzed specifically to measure the response that was achieved to the HA head and stalk regions of the protein. The serum will be tested against rescued influenza viruses that express chimeric HA proteins to differentiate the responses. Additionally, there is continued work going forward to generate similar particles based on a group 2 H3 HA protein. The broadly neutralizing activity will

likely not be cross group reactive, so a bivalent vaccine will likely be necessary to produce a truly universal influenza vaccine.

CHAPTER 3. STRAIN SPECIFIC IMMUNOGENIC RESPONSES TO RESPIRATORY SYNCYTIAL VIRUS FUSION PROTEIN DEPEND ON SITE Ø SPECIFICITY

3.1 Introduction

Respiratory Syncytial Virus (RSV) is the leading cause of bronchiolitis and pneumonia in infants[71]. Synagis© is the only licensed treatment available. It is a prophylactic antibody that requires monthly injections, thus limiting its use to extremely high-risk patient groups and making the widespread adoption of such a treatment unlikely. Given these statistics it is alarming that there is still no licensed vaccine available. This is due in part to the propensity of anti-RSV antibodies to lead to antibody-associated disease enhancement when the antibodies generated in response to the vaccines does not achieve the necessary titer or specificity for protection[72,73]. Efforts to boost titer to circumvent ADE are challenging because one of the main target groups for immunization is pregnant women, which necessitates developing a vaccine without using an adjuvant. Still, recent developments in understanding the immune response to RSV and protein engineering developments have given new insights and tools to develop the next generation of potential RSV vaccines.

The two major antigens on RSV are the surface glycoproteins F (fusion protein) and G (attachment protein). Of the two, the F protein is more conserved from strain to strain, and thus is the focus of many vaccine development efforts[74,75]. The F protein exists in two conformations on the surface of the virion, the metastable prefusion conformation (preF), and the stable postfusion conformation (postF)[75,76]. There is a vast conformational

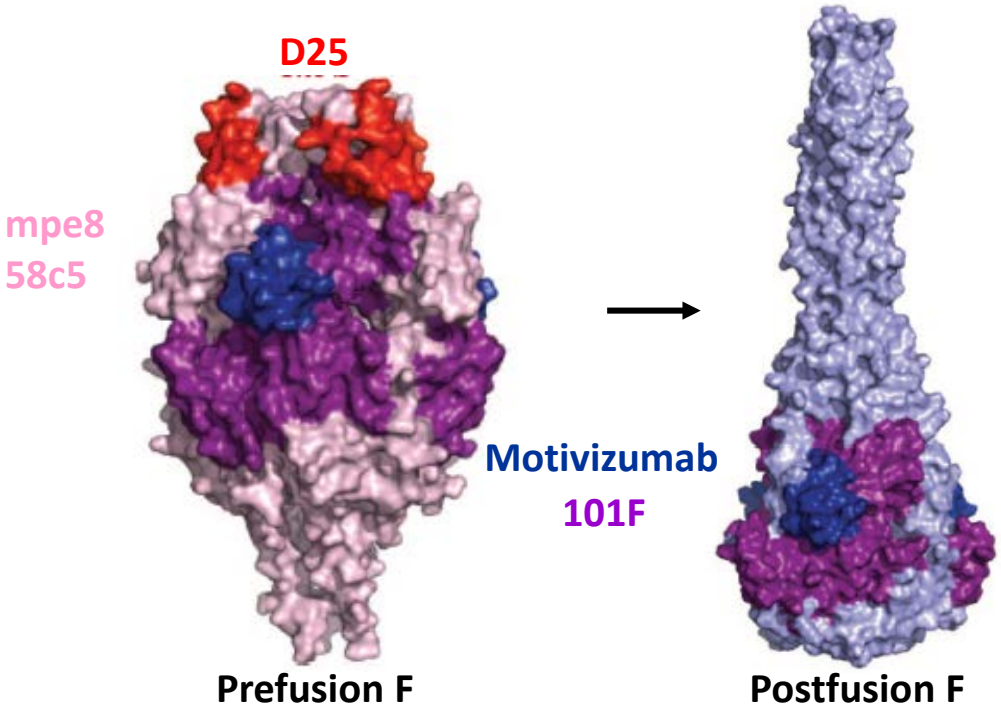

Figure 14. Crystal Structures of RSVF. RSFV prefusion and postfusion conformations from (refs). The dark purple and dark blue surfaces are conserved on both conformations, while the pink and light blue regions are specific to each conformer. The epitopes for several antibodies are also pointed out. D25, mpe8, and 58c5 bind only to the prefusion protein, Motivizumab and 101F bind to both conformers.

shift from preF to postF. Only 50% of the solvent exposed protein surface area is conserved between the two conformers[76]. Recently, McClellan et al. engineered an RSV F protein that is stable in the prefusion conformation[77]. This allowed Ngwuta et al to determine that over 90% of neutralizing antibodies to RSV found in human sera are specific to preF, whereas only 10% are specific to postF[76]. Interestingly, over 45% of these neutralizing antibodies are specific for a single antigenic site Ø that is found at the membrane distal region of preF. Thus, new attempts to develop an RSV vaccine are focused on generating antibodies to preF and specifically to antigenic site Ø.

Our work in this area is twofold. First, we hypothesize that we can increase the immunogenicity of RSV preF to generate high titers of antibodies that will neutralize RSV. Secondly we are interested in probing the importance and efficacy of antigenic site Ø. Antigenic site Ø is the most variable region of the F protein[78]. Excluding site Ø, RSV F protein has 94% homology across strains. Within protein F, the homology is only 77%[78]. Our hypothesis is that antibodies to site Ø are less likely to bind to and neutralize disparate strains of RSV than are other prefusion-specific antibodies that bind to other regions on preF. We have generated vaccine constructs that present two versions of stable preF: the wild-type protein, and a mutant protein that has 3 inserted glycosylation sites within antigenic site Ø (glycan KO)[76]. This mutant inhibits antibody binding, to site Ø and we hypothesize that it will also inhibit the generation of antibodies against site Ø. These vaccine constructs will allow us to test the broadly neutralizing activity of site Ø antibodies generated from a preF vaccine construct.

3.2 Materials and methods

3.2.1 Expression of Antibodies and RSVF

DNA coding for Sc-tm RSVF[79] and the variable domains of anti-RSVF antibodies was optimized for human expression and synthesized by Genscript. RSFV DNA was cloned into pcDNA3.1 between NcoI and XhoI with a leader peptide to direct the protein into the solution media. Site directed mutagenesis was performed as needed to generate mutant proteins using the Q5 SDM kit (NEB). Antibody DNA was cloned into the TGEX vector series per the manufacturer's protocol (company name). All proteins were expressed in HEK293F cells using the Expifectamine transfection kit. Strep-tagged (streptag II) RSVF was purified by affinity purification on a GE HiStrep column followed by SEC on a GE Superdex 200Increase 10/300 column. Antibodies were purified over protein A resin.

3.2.2 ELISA analysis

RSVF proteins were coated overnight at 4^{o}C, 0.1 µg/well in 50 mM carbonate buffer, pH 9.6 on Nunc Maxisorp plates. Wells were blocked for 1 hr at RT with 5% BSA in PBS-tween, washed, and primary antibodies were added at appropriate dilutions in 1% BSA in PBS-tween for 1 hr. HRP-linked secondary antibodies were used for detection.

3.2.3 Vaccine construct assembly

RSVF proteins were expressed as described[79] with a C-terminal spytag peptide incorporated. Azide-containing Spycatcher protein (Az-SpCat) was expressed in E. coli and purified using IMAC. After purification, Az-SpCat was reacted in excess to a 4 arm 20 kDa PEG molecule. PEGs with 3-4 Az-SpCats attached were purified by SEC and concentrated. Excess RSVF was added and allowed to react overnight at 4^{o}C. Final vaccine constructs were purified by SEC before being used in immunizations.

3.2.4 Immunization

Immunizations were carried out by ProSci, Inc. In short, 2 µg RSVF protein adjuvanted with Addavax (Invivogen) was injected subcutaneously into mice at days 0, 14, and 28 and mice were terminally bled on day 35. Final injection volumes were 80 µl per injection. Immediately prior to each injection, serum was collected for analysis. Each vaccine group was tested on n=5 BALB/C mice, 6-8 weeks old.

3.2.5 Serum analysis

First test bleed serum will be pooled from each group and all serum samples will be split in two, have being left and half being depleted of non-site Ø antibodies as described previously[76]. Resulting control and depleted sera will be tested for ELISA titer to RSFV glycan KO and the RSVF B Site Ø mutant proteins. Further serum analysis for titer and neutralization efficacy against full RSV viral strains will be performed in the labs of our collaborator according to previously described methods.

3.3 Results

3.3.1 Expression of RSVF and Glycan KO proteins

RSVF proteins were expressed through transient transfections into mammalian HEK 293F cells. Untagged proteins were purified from the cell supernatant by cation exchange x`chromatography followed by SEC. Streptagged proteins were purified by replacing the cation exchange step with a sreptactin column. Figure 15 shows the expression of both the wild type and glycan knock out (glycan KO) versions of RSVF. There is a slight MW change seen in SDS-PAGE indicating the glycosylations successfully

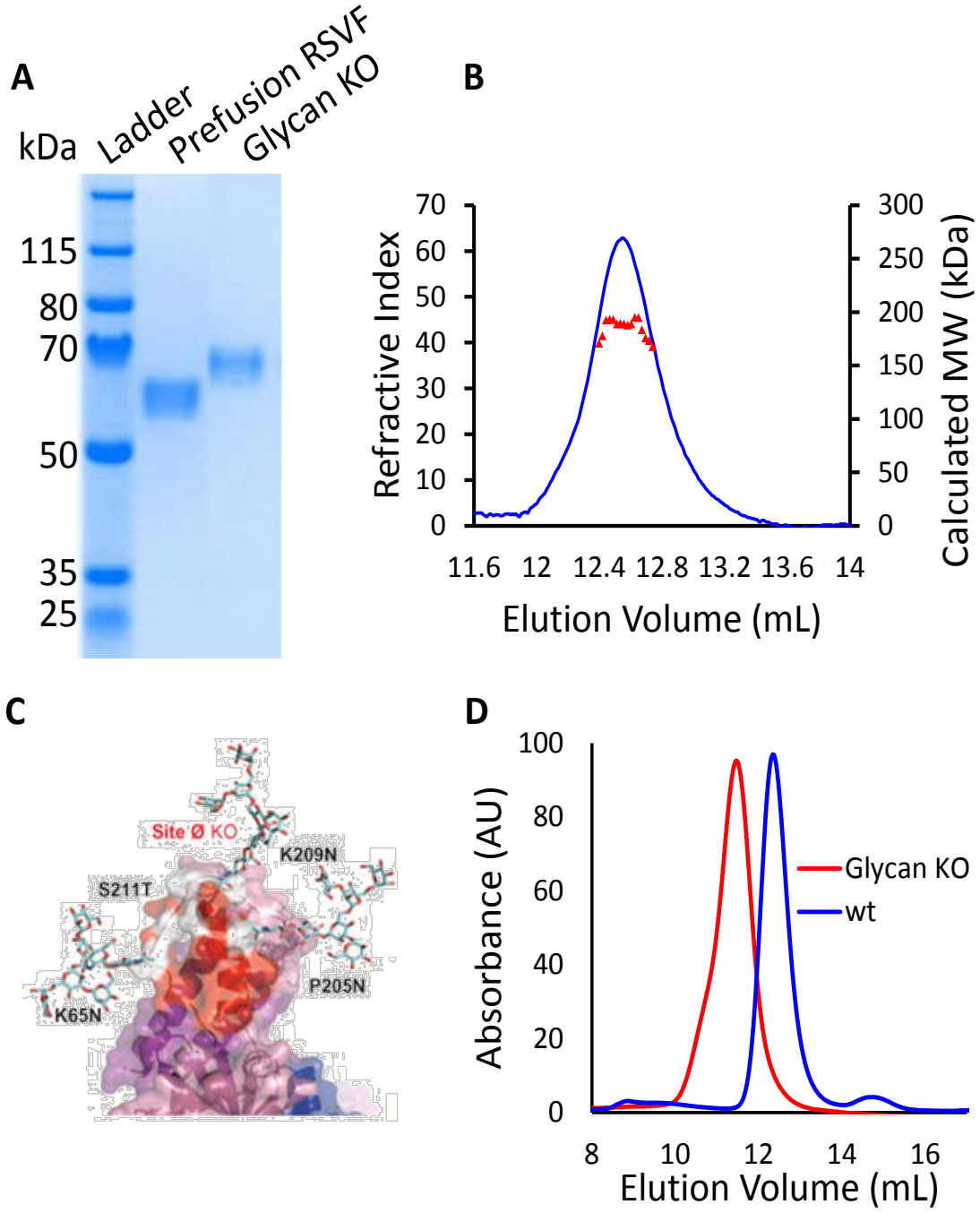

Figure 15. Expression of RSV preF. (A) SDS-PAGE of purified RSVF proteins, both the wild-type prefusion RSVF (wt RSVF) and the Site Ø glycan knockout mutant. Reprinted with permission from MacMillen Publishers, Ltd. (B) SEC-MALS of wt RSVF showing the assembly of the trimer. (C) Modeled image of glycan mutations added to Site Ø to block antibody binding, from Ngwuta, et al. 2015[76], reprinted with permission. (D) The glycan mutant showed a shift in MW (See panel A), which also showed a shift in the SEC elution profile from the wt protein.

occurred. SEC-MALS was used to verify the presence of the trimeric species. Figure 15C shows a model of the glycosylated protein showing how site Ø is blocked by the attached glycans. Lastly, the glycans make a steric difference on the surface of the trimeric protein as seen in the SEC chromatograms that the glycan KO elutes before the wtRSVF.

3.3.2 Expression of antibodies against RSVF

In order to probe the correct folding of the expressed RSVF, as well as analyse the serum responses to the vaccines developed, we expressed several antibodies to RSVF. The antibody epitopes are shown in Figure 14. The antibodies were purified over protein A resin, and an SDS-PAGE gel of the antibodies is shown in Figure 16 and were used in further ELISAs for testing RSVF.

3.3.3 ELISA analysis of RSVF proteins

RSVF proteins were coated on ELISA plates and probed for binding to each of the expressed antibodies. wtRSVF bound to all antibodies showing that it is correctly folded (Figure 17). Glycan KO RSVF bound to all antibodies other than D25, showing that is it both correctly folded and that it sterically inhibits antibodies from binding to site Ø. Additionally, added purification and conjugation peptide tags to the C-terminus of the protein did not alter antibody binding.

3.3.4 Expression and analysis of an RSVF B site Ø protein

As was mentioned earlier, site Ø is the most variable region of RSVF. Figure 18 shows the compared sequences of RSVF A2 and an RSVF B strain within the site Ø epitope. Six residues are different between the two strains, and of them, three residues directly contact the site Ø antibody D25. We expressed a version of RSVF that had only the site Ø epitope

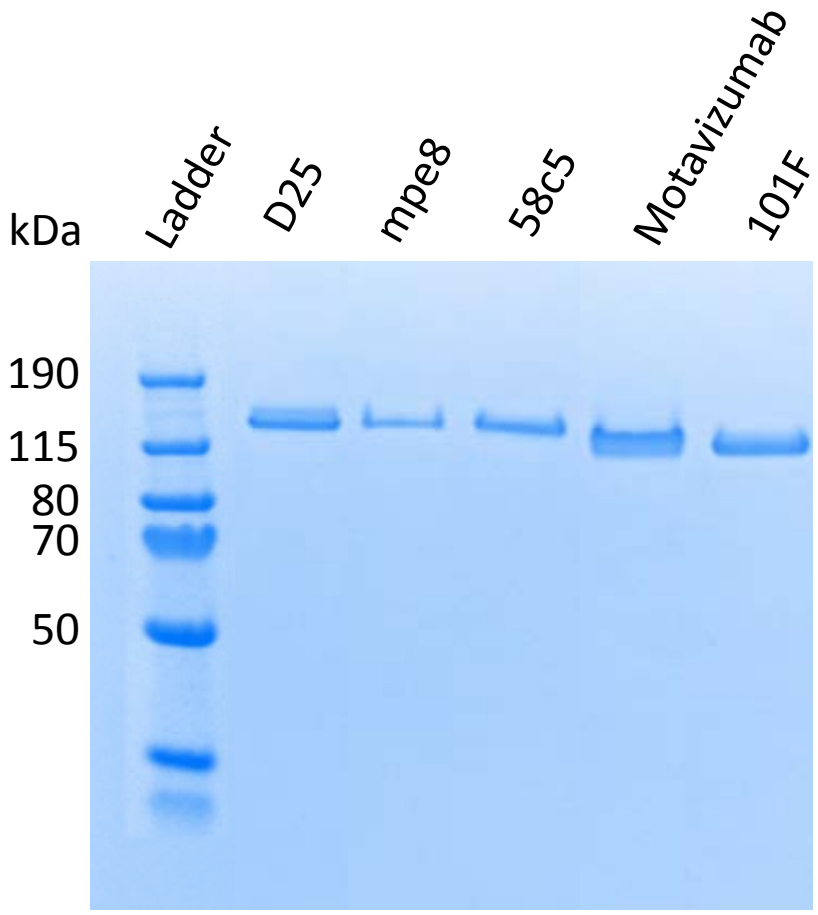

Figure 16. RSVF antibody expressions. SDS-PAGE of antibodies expressed to bind to RSVF. The antibodies expressed are the same ones that were highlighted in Figure 14.

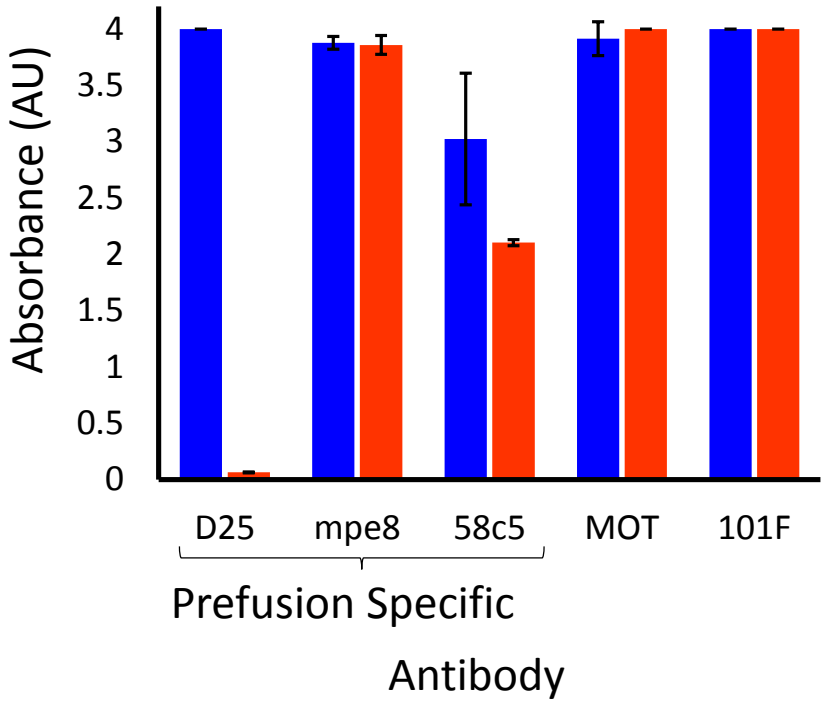

Figure 17. ELISA of RSVF proteins. Expressed RSVF proteins were coated and probed with RSVF antibodies. Blue bars: wtRSVF binding. Red bars: glycan KO binding. Glycan KO binds to all antibodies other than D25, which binds to site Ø.

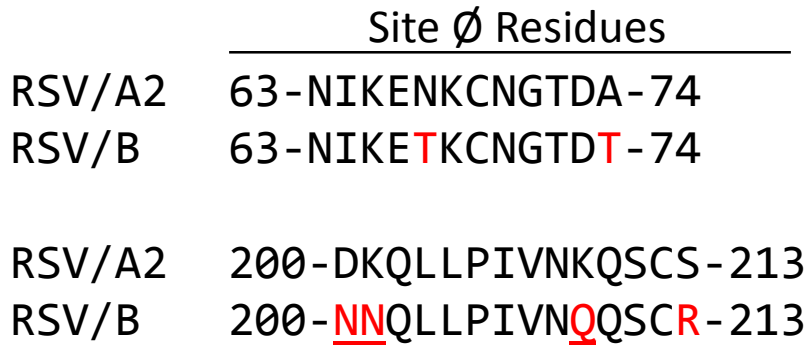

Figure 18. Variability within Site Ø. The sequences of the Site Ø epitope in RSV/A2 and RSV/B are compared. Red residues are in the RSV/B sequence differ from those in RSV/A2, and underlined residues come into direct contact with the neutralizing antibody D25.

mutated to the RSVF B strain sequence. The expressed B site Ø protein bound in ELISA to Motivizumab (Figure 19; all other non-site Ø antibodies bound B site Ø RSVF, data not shown). However, the protein showed a markedly lower affinity for site Ø antibodies D25 and AM22 than the wild-type protein. This result encouraged us to hypothesize that generated site Ø-directed antibodies in a typical antibody response will not be as effective at cross strain protection as those generated specifically against epitopes other than site Ø.

3.3.1 RSVF vaccine design and assembly

RSVF vaccines were designed based on the spycatcher-spytag conjugation strategy[67]. Illustrated in Figure 20, the spycatcher protein forms an isopeptide bond with the spytag peptide that can be attached to a protein. We conjugated spycatcher to a 4-arm PEG molecule via a dibenzylcyclooctyne (DBCO)-Azide reaction. The spycatcher proteins were expressed with the mutation T56pAzF, to add an aizide moiety on the opposite site of the reactive lysine. The PEG-spycatcher scaffolds were then mixed with RSVF and the fully conjugated vaccine was purified by SEC. We were able to purify a mixture of 3 and 4 spycatchers per PEG molecule and thus the final vaccine construct was comprised of molecules with 3-4 RSVF trimers on them. We generated vaccines using wtRSVF and Glycan KO RSVF, as well as a control vaccine composed of the scaffold alone.

3.3.2 Immunizations and Serum analysis

Immunizations are currently underway by ProSci, Inc. We will assess the binding and neutralization activity of both the full serum samples and serum that has been depleted of all anti-RSVF antibodies other than those to site Ø. The serum depletion test has been reported previously using the Glycan KO RSVF to pull down all non-site Ø-binding

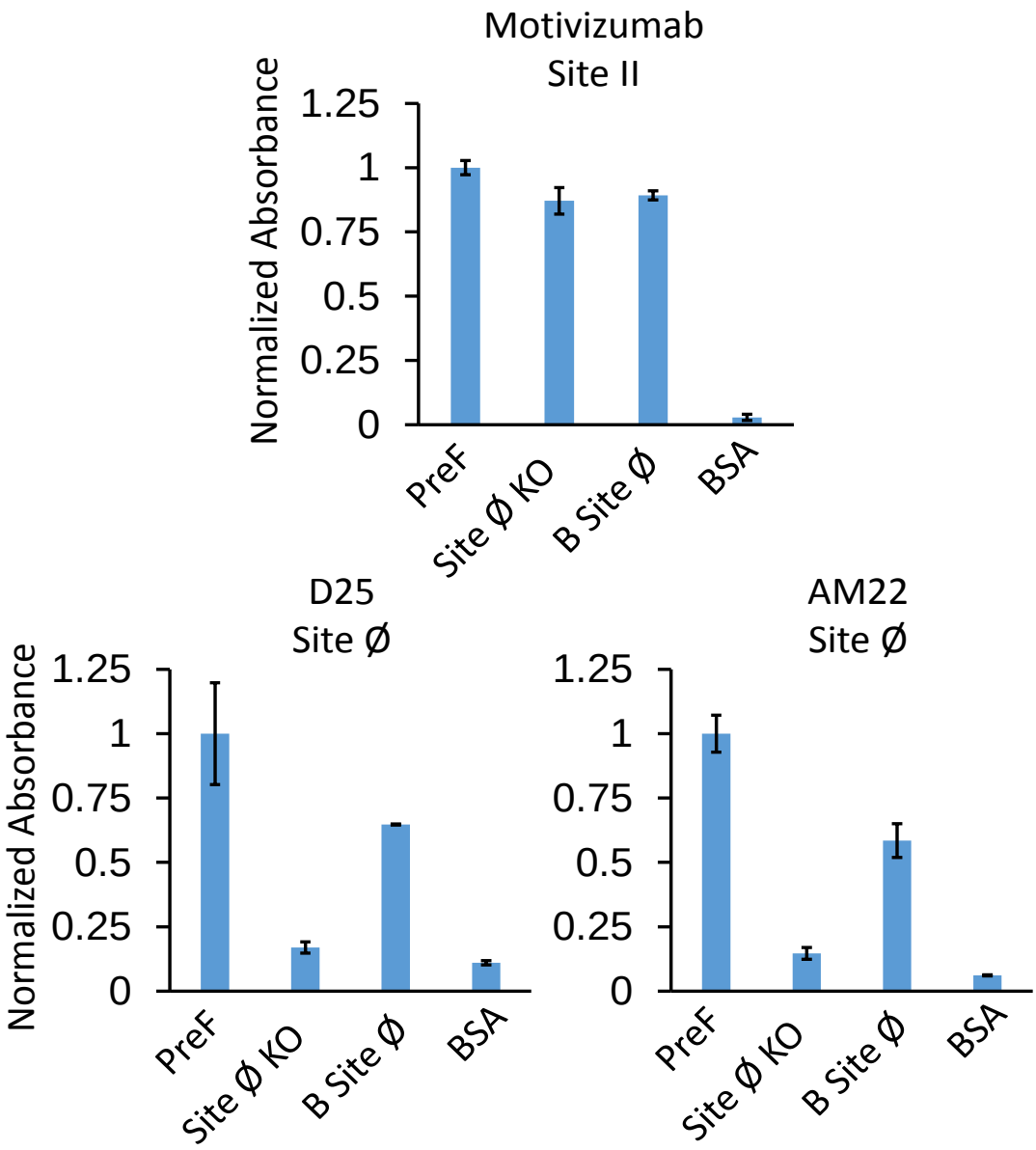

Figure 19. RSVF-B Site Ø mutations block Site Ø antibodies. RSVF-B Site Ø was probed by three prefusion specific antibodies. Site Ø specific antibodies have a significant reduction in binding to B Site Ø.

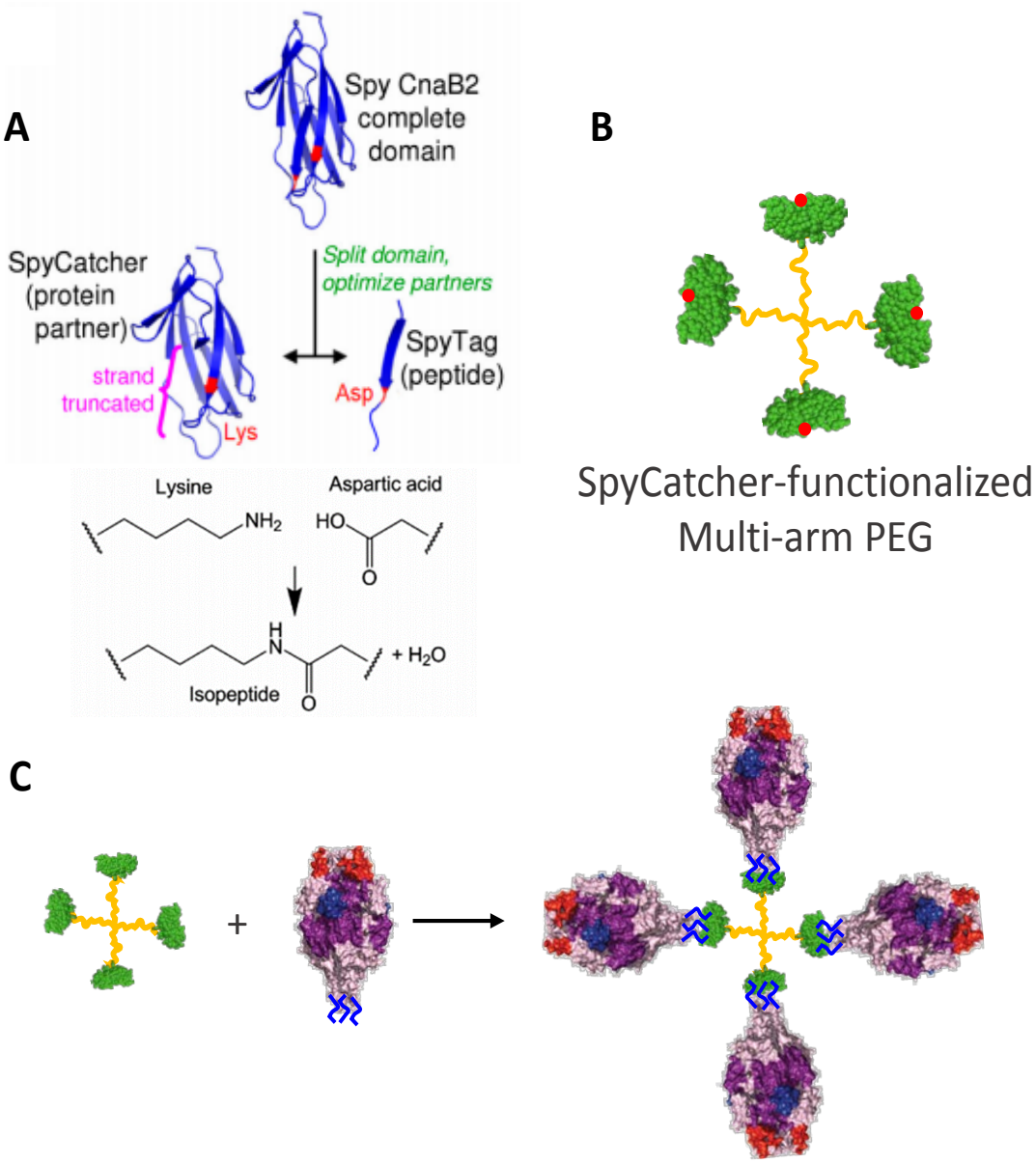

Figure 20. RSVF vaccine design. (A) Vaccine scaffolds are based on the spycatcher-spytag system developed by Brune et al[67] (reprinted with permission). The spycatcher protein reacts with a spytag peptide to form and isopeptide bond. Adapted with permission from Brune et al. (B) The core of the vaccine is a DBCO activated 4-arm PEG molecule that is conjugated to spycatcher via an inserted pAzF residue opposite of the reactive face of the protein. (C) Final vaccine assembly was performed by mixing Spycatcher-PEG with spytagged RSVF (spytag represented in blue). The resulting molecule presents RSVF with site Ø at the surface, similar to viral presentation.

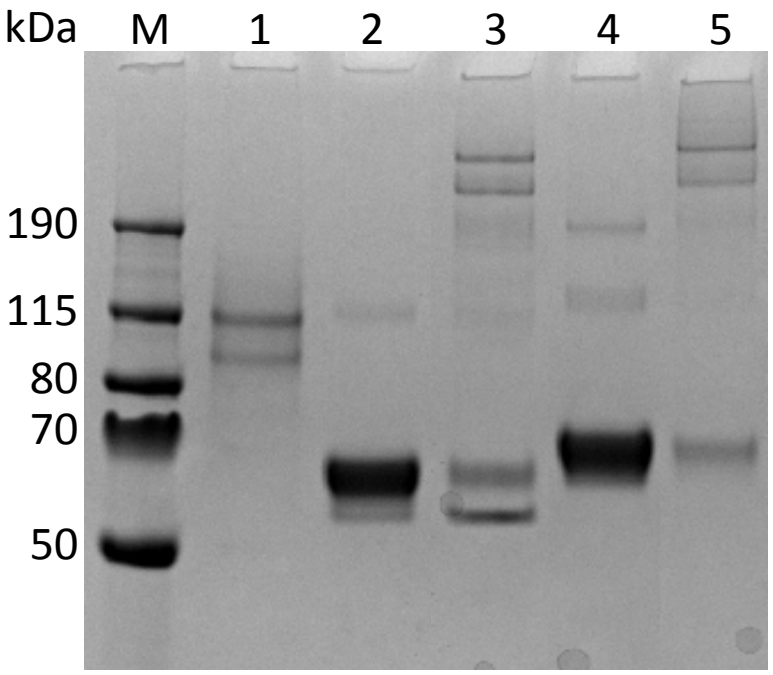

Figure 21. Protein Gel of RSVF vaccine assembly. Lanes: M – marker; 1 – Spycatcher+4-arm-PEG purified to a mixture of trimeric and tetrameric spycatcher protein; 2 – pure wtRSVF, 3 – purified wtRSVF vaccine with activated scaffold present, the ~60 kDa band results from the RSVF trimer disassembling under SDS-PAGE and is not soluble RSVF; 4 – pure glycan knockout RSFV; 5 – assembled vaccine of Glycan KO RSVF, showing the same pattern as the wtRSVF vaccine.

antibodies. We have done initial experiments to verify that the serum depletion assay will work. Firstly, we combined site Ø binding antibodies or non-site Ø binding antibodies to create a mock serum sample. These antibody mixtures were then depleted with glycan KO RSVF and assayed for residual binding (Figure 22A). The site Ø antibodies retained almost all of their binding, showing that site Ø antibodies will be retained in the depleted serum. Conversely, over 80% of the binding from non-site Ø antibodies was removed. To further verify our ability to perform a serum depletion test with immunized mouse serum, we depleted serum with reactivity towards GFP with soluble GFP in the same manner (Figure 22B). The serum that was not depleted or passed over a mock protein retained binding, whereas approximately 75% of the binding from antibodies was removed by the depletion step. These results make us confident that the serum depletion experiment with RSVF-reactive serum will work as well. We will initially test the ability of the serum generated to bind to the B site Ø RSVF mutant we have expressed. If the site Ø antibodies generated show decreased binding to the RSVF/B sequence, we will then work with our collaborators at Emory University to assay for titer and neutralization activity against a library of RSV strains.

3.1 Discussion

The generation of an effective RSVF vaccine would be an effective way to decrease the disease burden that RSV causes, especially in newborn infants. Our work has been meant to uncover the potential ramifications of focusing on generating an immune response specifically to site Ø. Antibodies that are less effective on diverse strains of the virus could lead to further antigenic drift or antibody mediated disease enhancement. By doing this study, we will be able to inform future RSV vaccine design efforts.

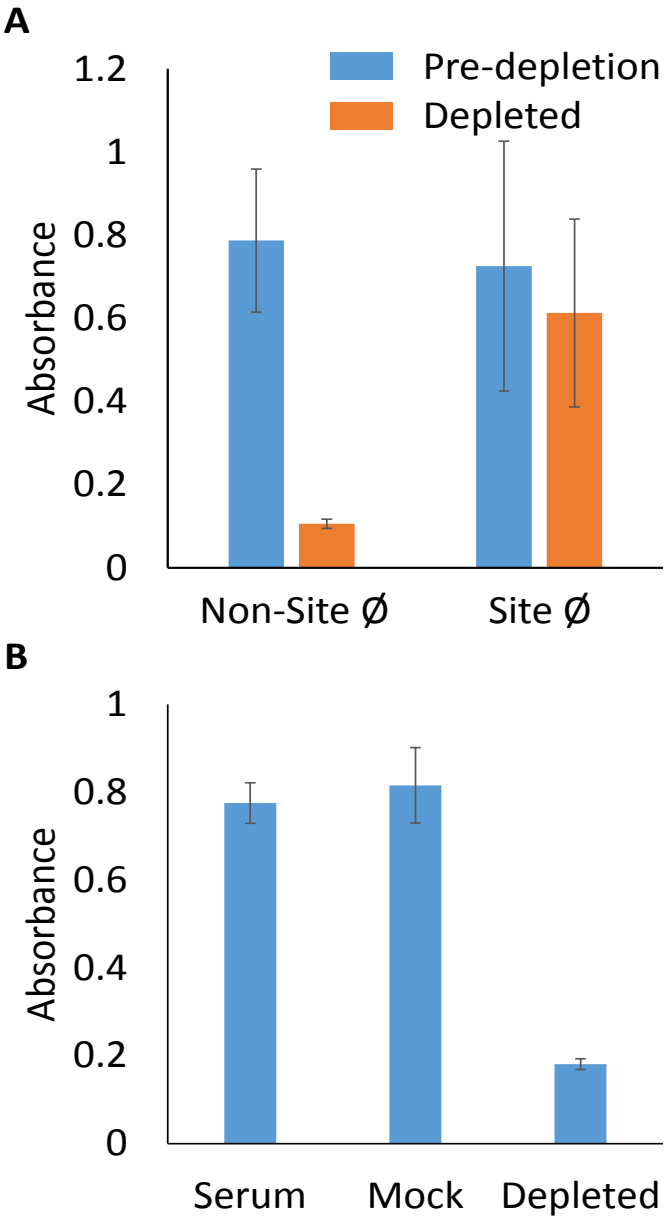

Figure 22. Serum depletion. (A) Two pools of antibodies that bind to RSVF were made; one of non-site 0 binders (101F, mpe8, Motivizumab) and one of Site 0 binders (D25 and AM22). Antibodies were depleted from the samples by exposing to site 0 KO RSVF and pulled down by magnetic beads. Over 80% of the non-site 0 antibodies were pulled down, while the Site 0 antibodies remained in solution. (B) Mouse serum that was reactive to GFP was diluted and exposed to GFP and pulled down with magnetic beads. Again, depleting the serum with GFP resulted in close to 80% of the antibodies being removed from the samples.

3.2 Future work

The vaccine scaffold used here was desirable because it allowed for covalent attachment of RSVF to the scaffolding molecule. Future work in this vaccine design space will be geared toward assessing the importance of the vaccine scaffold architecture in generating broadly neutralizing antibodies. Further, the insertion site of the spytag sequence is being looked at to see how the orientation of RSVF on the scaffold changes the antibody response generated.

CHAPTER 4. NANOPATTERNING SOLUBLE PROTEIN ANTIGENS TO GUIDE IMMUNE RECOGNITION TO DESIRED EPITOPES

4.1 Introduction

Vaccination remains one of the most effective methods to prevent disease. However, due to variations in pathogenic proteins and antigenic drift, several pathogens can evade the immune responses elicited by potential vaccines. It is becoming more and more clear that generating immune responses to specific regions of proteins that are highly conserved or show higher neutralization potential can potential circumvent a pathogen's route of immune evasion[76,80–83]. Consequentially, there exists a need to develop methods to refocus the immune response toward these desirable epitopes.

Glycosylation is used in nature to alter the immune response to antigenic proteins. This is well documented for both simian immunodeficiency virus and human immunodeficiency virus that have glycosylation patterns that shield neutralizing epitopes from the immune system[80,81]. Efforts to mimic this natural phenomenon include adding and removing glycosylation sites or changing the expression system to increase or reduce the size of glycan modifications[82,84]. Recently, Du et al. used site specific glycosylation to map epitopes on the MERS corona virus that are important for generating neutralizing antibodies[83]. However, there are limitations to using glycosylation for modulating protein antigens. First, this posttranslational modification is often vital for proper folding of proteins. Second, glycans themselves can become part of neutralizing epitopes[85]. Finally,

glycosylation is a blunt tool that does not allow for tailoring the structure of the glycans in a site-specific manner.

We therefore have developed a method for nanopatterning protein antigens that combines site-specific mutations with biochemical conjugation to shield desired protein epitopes. In short, non-cannonical amino acids can be inserted near a desired epitope to shield and then the protein can be directly functionalized with molecules such as PEG to shield the epitope. We have used this approach on a model protein, GFP, to illustrate the ability to refocus the immune response to specific epitopes.

4.2 Materials and methods

4.2.1 Protein expression and purification

DNA coding for superfolder-green fluorescent protein (sfGFP, PBD ID: 2B3P) and spycatcher (PDB ID: 4MLI) was optimized for expression in E. coli and synthesized by Genscript, Inc. (Carlsbad, CA) with a c-terminal hexahistidine tag. Spycatcher had an additional N-terminal streptag. The coding region was then cloned into a modified pet28b vector between the NdeI and XhoI cut sites with the n-terminal tag removed. Site-directed mutagenesis was performed using the Q5-SDM kit (New England Biolabs, Ipswich, MA). Primers were designed using the NEBasechanger tool. For expression of proteins not containing the amber codon, pet28b vectors were transformed in BL21(DE3) E. coli and grown at 37^{o}C in 2xYT media with 50 µg/ml kanamycin. Expression was induced by the addition of 1 mM IPTG at OD=0.5-0.9. After induction, the temperature was lowered to 30^{o}C and expression continued overnight. Pet-28b plasmids for expressing uAA containing proteins were co-transformed with pEvol-pAcFRS.2.t1 (a gift from Farren Isaacs, Addgene

plasmid #73544) to add the machinery to insert the unnatural amino acid (uAA) p-azidophenylalanine (p-AzF) in response to the amber codon. Cells were grown in 2xYT media supplemented with 50 µg/ml kanamycin and 50 µg/ml chloramphenicol. At OD=0.5-0.8, 0.02% L-arabinose and 1 mM p-AzF were added to induce the production of the uAA machinery, and at OD=1.3-1.5, 1 mM IPTG was added, and expression continued at 30^{o}C overnight. After expression, cells were pelleted by centrifugation at 4000xg for 30 min. Cell pellets were suspended in buffer A (50 mM Tris, 500 mM NaCl, 50 mM imidazole, pH 8) containing 1 mg/ml lysozyme and a protease inhibitor cocktail (S8830, Sigma Aldrich, St Louis, MO). After 30 min incubation at 4^{o}C, 0.1% deoxycholate was added and cells were lysed by sonication until no longer viscous. Cell lysates were clarified by centrifugation at 30,000 x g for 30 min at 4^{o}C. Clarified lysates were filtered through a 0.45 µm filter and mixed with Nickel-NTA resin (Pierce). After a 2-hour incubation at 20^{o}C, the slurry was added to a drip column and allowed to gravity drain. The resin was washed with 10 column volumes (CV) of buffer A, followed by 10 CV of buffer A with 100 mM imidazole. Purified proteins were eluted with 500 mM imidazole in buffer A. Eluted GFP proteins were buffer exchanged into PBS by spin filtering through a 10 kDa MWCO filter and concentrated prior to storage in the dark at 4^{o}C. Eluted spycatcher proteins were then loaded onto a streptactin column (GE Healthcare), washed with 20 CV binding buffer (100 mM Tris, 150 mM NaCl, 1 mM EDTA) and eluted with 2.5 mM desthiobiotin in binding buffer. Purified spycatcher was buffer exchanged and concentrated through a 3 kDa MWCO filter and stored at 4^{o}C until further use.

4.2.2 PEGylation and purification

GFP double mutant contained p-AzF at residues 131 and 209. Gfp triple mutant contained p-AzF at residues 34, 109, and 200. SPycatcher-Az contained the mutation T56Az. p-AzF containing proteins were mixed at >10 mg/ml with excess (5-10 molar excess) 2 kDa mPEG-DBCO (Nanocs, New York, NY) and left to react overnight at room temperature or at 4^{o}C for >48 hrs. PEGylated GFPs were purified by native gel electrophoresis. After running, bands were excised and protein was eluted by placing the excised band in PBS and letting it rock at 4^{o}C overnight. Soluble protein was then concentrated as before. Spycatcher-PEG was purified by SEC on a GE Superdex 200 prepgrade 16-60 column, eluted in PBS. All proteins were confirmed to have PEG by SDS-PAGE and MALDI-TOF mass spectrometry. Final Pegylated proteins were isolated in pBS by elution through a GE Superdex 75 10/300 SEC column.

4.2.3 Purification of protein tagged GFP

Spycatcher-PEG was mixed with excess spytagGFP containing an inserted spytag and spacer (GSGGSGGSGGSGAHIVMVDAYKPTKGSGGSG) after residue 52. After overnight incubation at 4^{o}C all spycatcher PEG was consumed and the mixture was passed over a streptactin column to remove unreacted spytagGFP. This protein-conjugate was finally purified by SEC on a GE Superdex 75 10/300 column.

4.2.4 Immunizations

Immunizations of GFP related proteins were carried out by ProSci, Inc. (Poway, CA). In brief, protein antigens were diluted to 75 µg/ml prior to sending to ProSci. On days 0,14, and 28, 3 µg of antigen were injected adjuvanted with Addavax. On day 35 mice were bled and serum was kept for analysis.

4.2.5 Serum analysis

Mouse serum to GFP will be assessed for endpoint titer against wtGFP. and other GFP mutant proteins to assess site specific-reactivity of the antibodies. In short, GFP proteins will be captured onto streptavidin coated ELISA plates via a site-specific biotinylation with DBCO-Biotin.

4.3 Results

4.3.1 Selecting PEG conjugation parameters

We used PEG as an initial test to validate our ability to shield protein epitopes from the immune system and redirect the immune response. We first identified epitopes on GFP that had been previously used as immunogens for commercially available antibodies. Figure 23 shows the epitopes on GFP that were identified. For proof of principle, we chose epitope 1 as the region that we would try to either block or direct the immune response toward. For blocking, the selection of residues was based on solvent accessibility of the sidechain and proximity to the epitope. To ensure that the antibody blocking effects seen were directly related to the shielding effects and not to the unnatural amino acid incorporation, we selected residues to mutate that were near but not within the specified epitope. For directing the immune response toward the epitope, we selected solvent accessible residues distant from the epitope that were evenly spaced to allow shielding of the non-epitope surface of the protein.

The size of PEG was selected based on the root-mean-square (RMS) end-to-end distance. We selected 2 kDa PEG to use for this initial study because it corresponds to an RMS

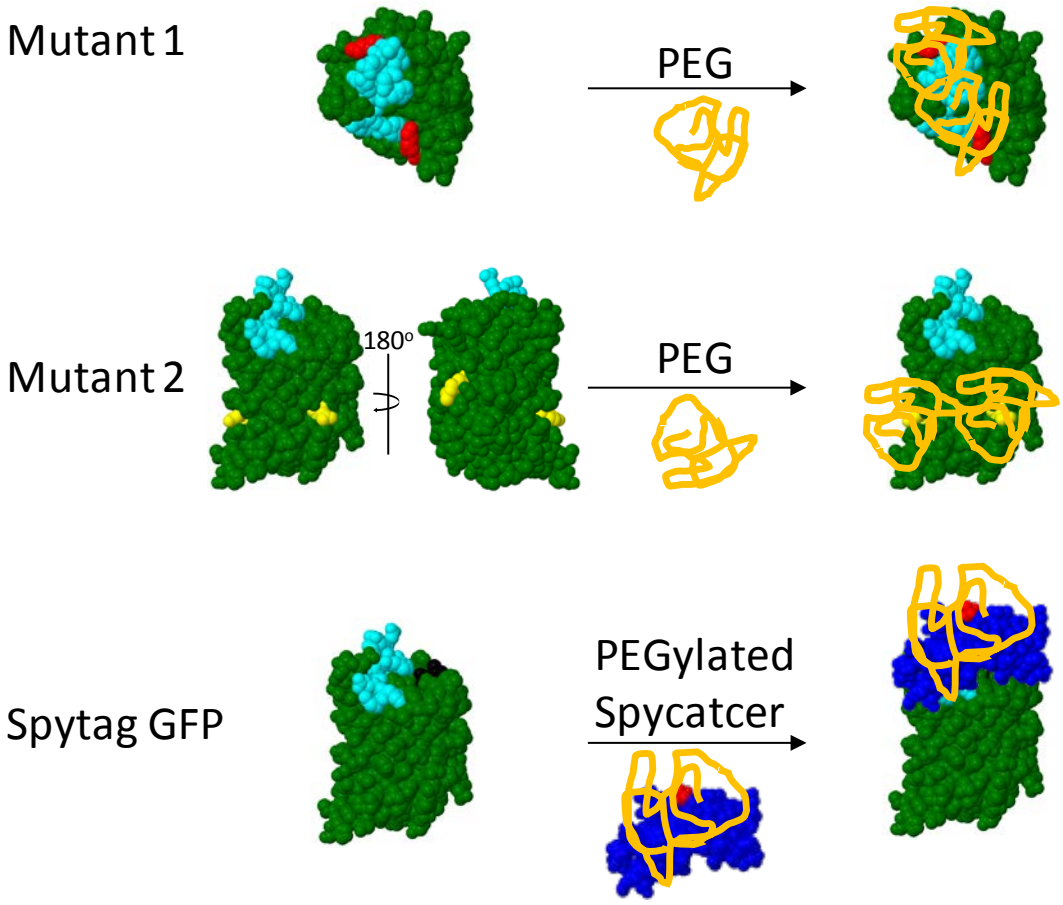

Figure 23. Selecting mutants for site specific bioconjugation. Mutant 1 was designed to shield the highlighted epitope (cyan). Residues K131 and K209 (red) were mutated to p-AzF and conjugated to 2 kDa mPEG-DBCO. Mutant 2 was designed to guide the immune response toward the highlighted epitope by shielding distant regions with PEG (E34pAzF, R109pAzF, and Y200pAzF in yellow). Spytag GFP also blocks the highlighted epitope with an inserted Spytag peptide (between K52-E53, black) that reacts with a PEGylated spycatcher protein.

distance of 4.2 nm[86] and thus can feasibly shield epitopes without covering the entire surface of the protein.

4.3.2 Expression, purification, and PEGylation of proteins

Amber stop codons were inserted into GFP at the desired codons, and the protein was co expressed in E coli with plasmid pEVOL-pAzRS2.t1[87] for the incorporation of p-azidophenylalanine (p-AzF). The purified full length protein was then reacted with excess mPEG-DBCO. The small length of PEG made purification of the final PEGylated protein by chromatography difficult. Instead, we chose to use native polyacrylamide gel electrophoresis (PAGE) to separate differently PEGylated proteins on the basis of the altered m/z ratio. Figure 24 shows an example image of a PEGylated reaction mixture after separation by native PAGE. After excising the band, we were able to obtain fully PEGylated proteins to be used as immunogens. Figure 25 shows an SDS gel showing that both non-PEGylated and PEGylated proteins were purified to homogeneity before proceeding with immunizations. The addition of PEG was verified by MALDI-TOF mass spectrometry, and an example result is depicted in Figures 26-27. The MW of non-pegylated GFP is close to 27.7 kDa, and after the addition of 2 or 3 2kDa PEG molecules, the mass shifts correspondingly.

4.3.3 Elisa analysis of protein antigens

Purified proteins were then coated on ELISA plates and probed with antibodies binding to the specified epitopes (Figure 28). Non-PEGylated wild type and mutant proteins bound to all antibodies. As shown in Figure 28, the doubly PEGylated mutant designed to block epitope 1, blocks antibody 1, while it does not block antibody 2. The

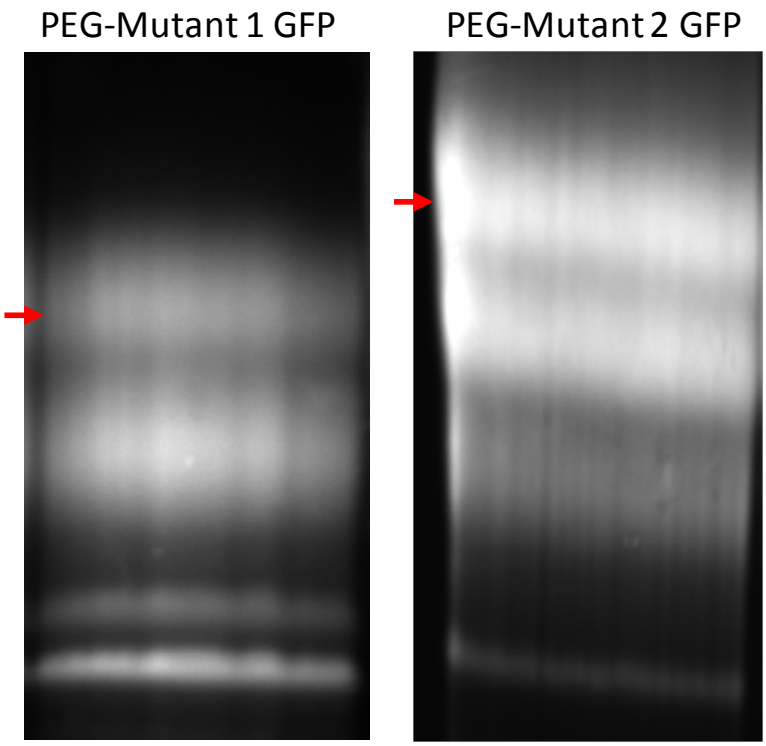

Figure 24. Native-PAGE Separation of PEGylated GFP. PEGylated GFPs were separated by Native-PAGE. The indicated bands, corresponding to fully PEGylated GFP were excised and processed as GFP antigens.

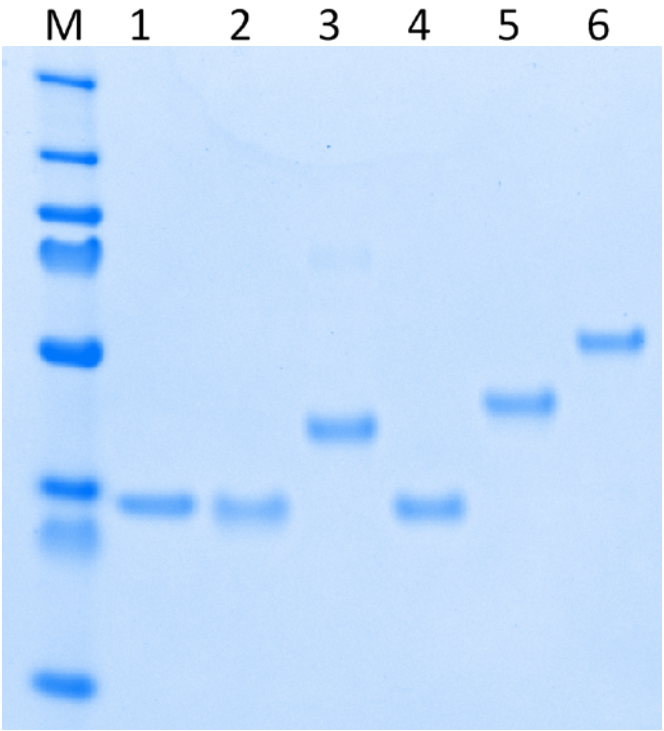

Figure 25. SDS-PAGE of GFP antigens. Lanes: (M) Marker, (1) wild type GFP, (2) Mutant 1 GFP – K131pAzF+K209pAzF, (3) PEGylated Mutant 1 GFP, (4) Mutant 2 GFP – E34pAzF+R134pAzF+Y200pAzF, (5) PEGylated Mutant 2 GFP, (6) GFP-PEGylated Spycatcher fusion protein.

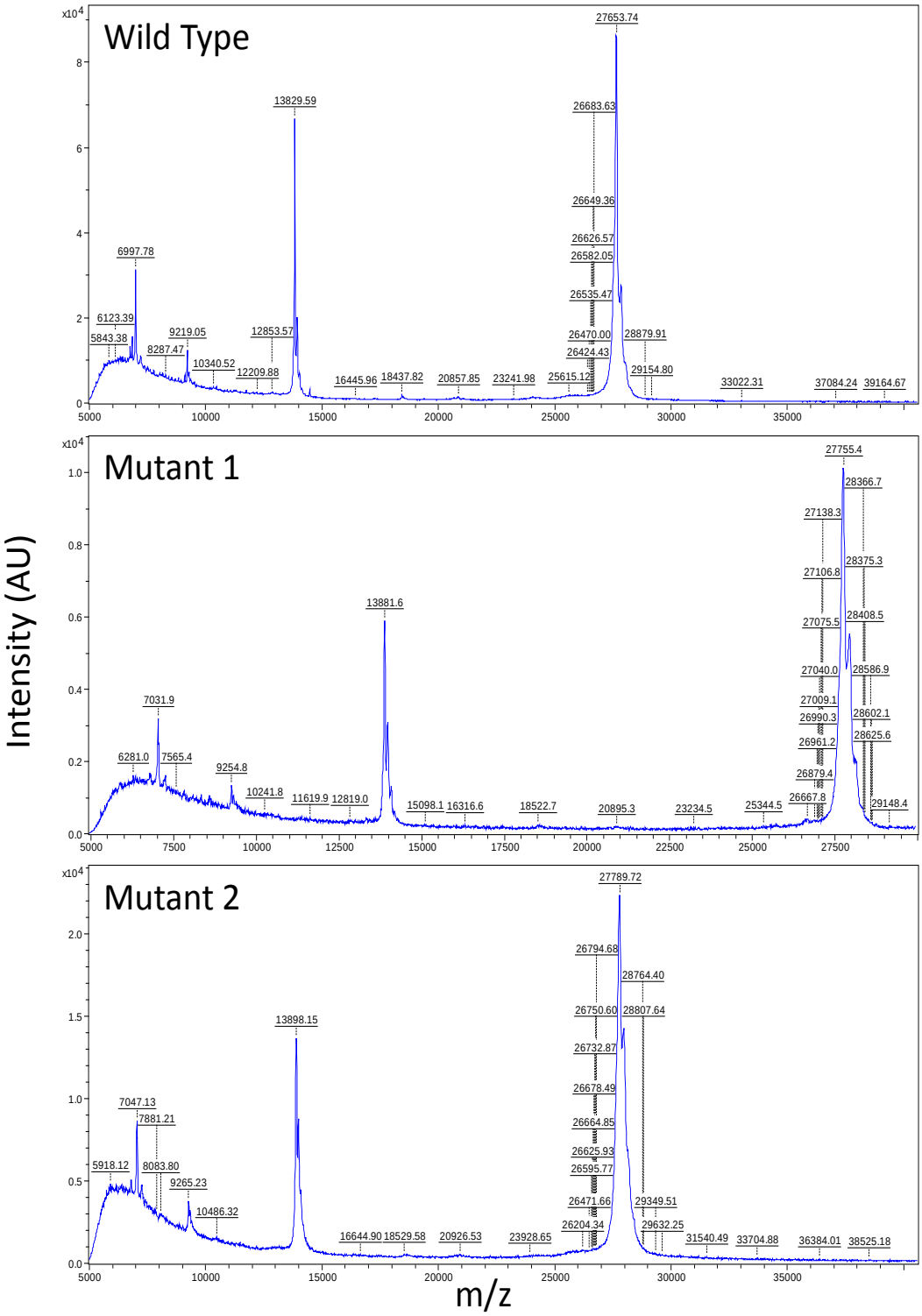

Figure 26. MALDI-TOF spectra of non-PEGylated GFP antigens. wtGFP, Mut1 and Mut2 were analyzed by MALDI-TOF to confirm insertion of the pAzF residues. The increase in MW of the mutants corresponds to the replacement of the mutated residues with pAzF.

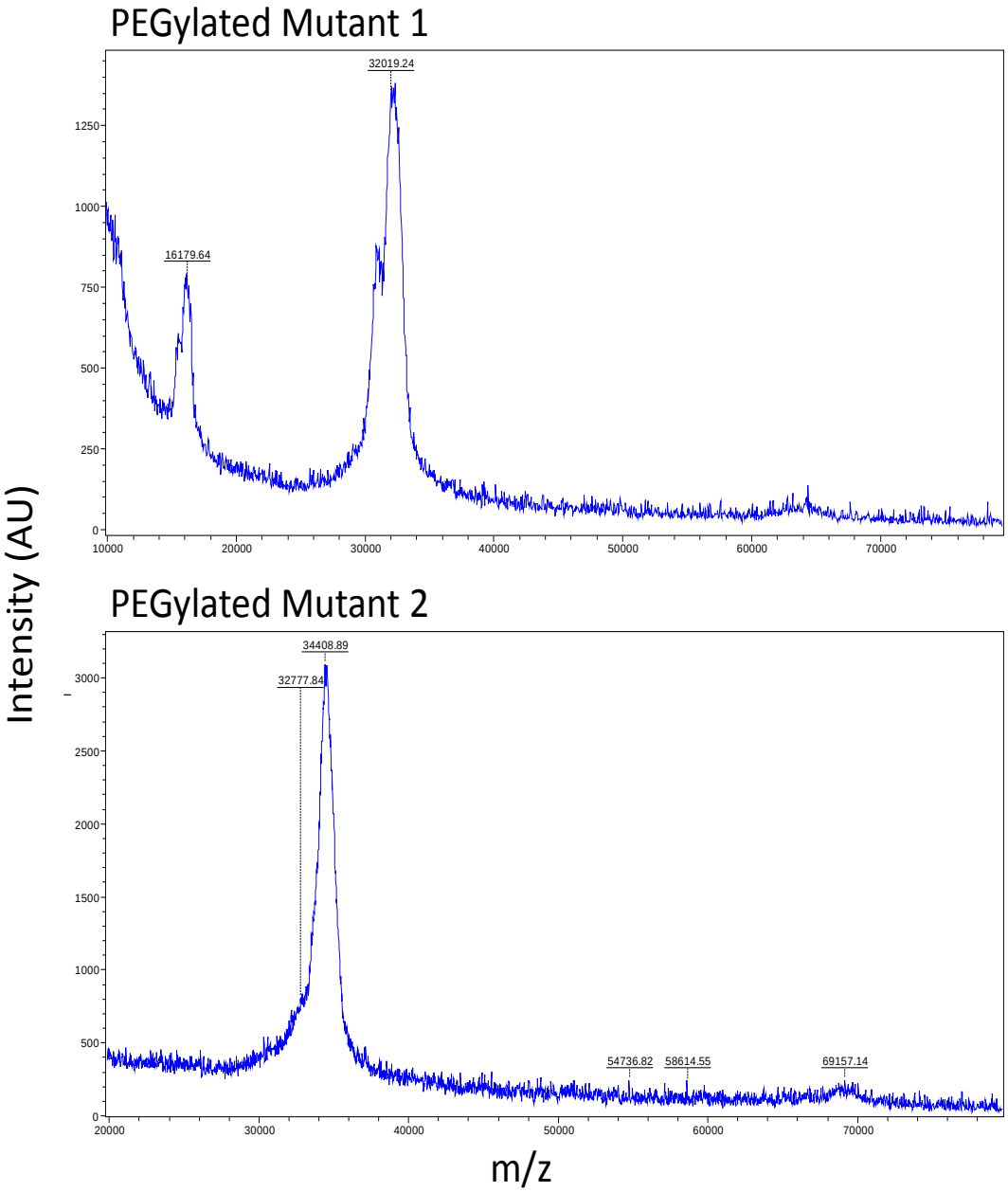

Figure 27. MALDI-TOF spectra of PEGylated GFP antigens. PEGylated GFP mutants after purification were submitted for mass psec analysiss. The broad peak coris a result of the polydispersity of the PEG molecules, but the large 2 kDa shiftseen between PEGylated mutant 2 (MW: ~32kDa) and PEgylated mutant 2 (MW ~34.4 kDa) indicates that the PEGylation was successful. The lower MW shoulder is a result of trace amounts of n-1 PEGylated product not fully removed by purification.

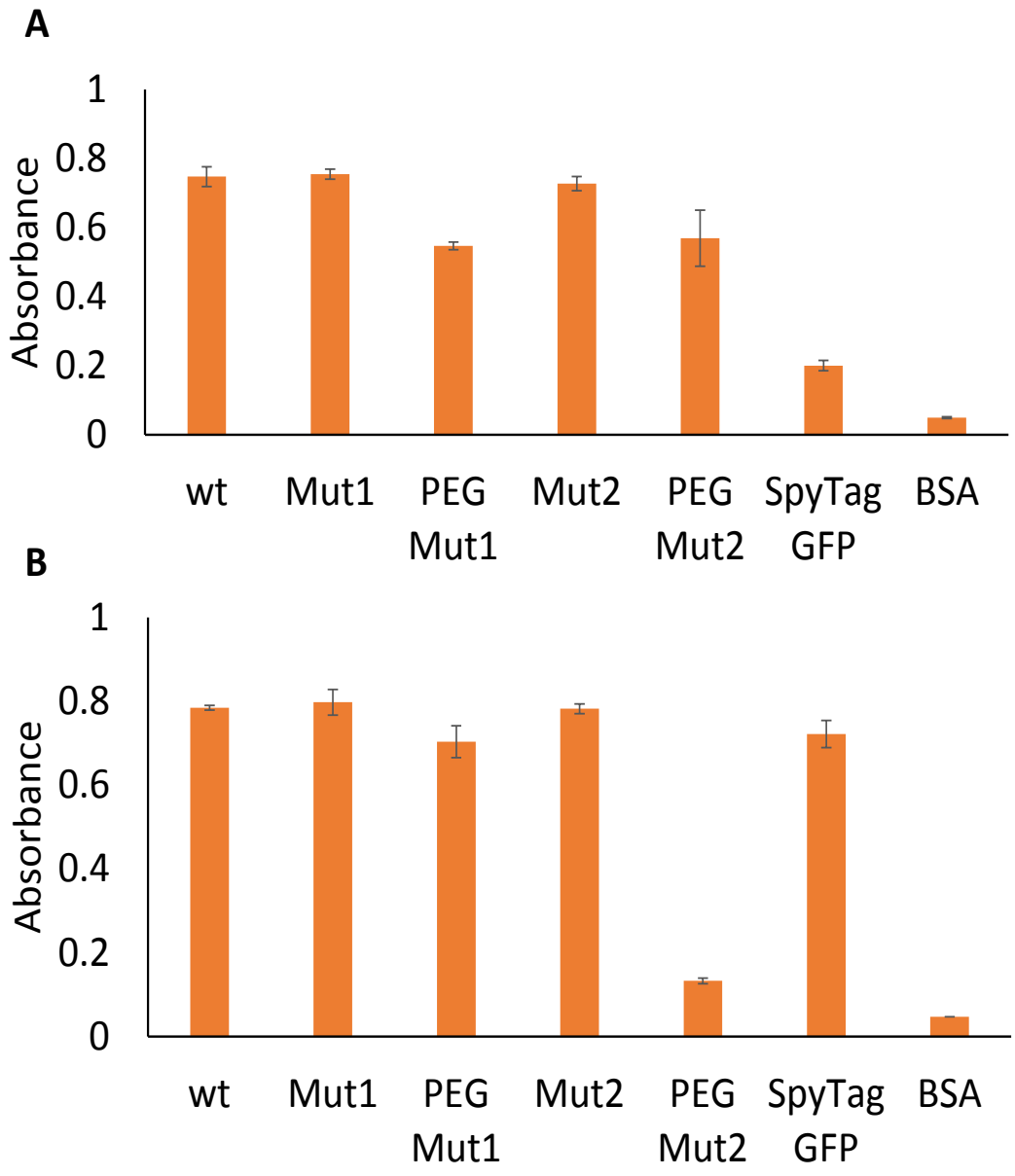

Figure 28. GFP antigens selectively bind to antibodies. (A) GFP antigens were coated on ELISA plates and detected with antibody GSN149 that binds to the cyan highlighted epitope depicted in Figure 23. The PEGylated proteins marginally inhibit antibody binding, whereas the Spytag GFP largely inhibits antibody binding. (B) GFP antigens were also detected with an N-terminal binding antibody that binds to a distal region of the protein from the GSN149 binding site. The PEGylated mutant 2 protein is the only antigen that blocks this site.

triple PEGylated protein does not block antibody 1, but does block antibodies 2 and 3. These ELISA results showed us that the PEGylated proteins did have the potential to alternatively block and direct an immunological antibody response to epitope 1.

4.3.4 Immunization and serum analysis

Serum from each mouse was collected prior to each injection, and one week following the final injection. Data is still being collected but we have analysed the serum from wtGFP and Spytag GFP for titer against wtGFP. Figure 29 shows that the overall antibody titer to wtGFP is the statistically the same after immunizations with wtGFP or spytag GFP. The antibody response to spycatcher is significantly lower than to wfGFP. This is likely caused by the direct PEGylation of the spycatcher protein, thus lowering its immunogenicity. As the serum returns from immunizations we will test the reactivity to wtGFP as well as to site-specifically immobilized GFP. The results from these tests will enable us to verify that nanopatterning does enable us to direct the immune response.

4.1 Discussion

We have developed an approach to nanopattern protein antigens to shield specific epitopes from the immune response. This approach is orthogonal to glycosylation and as such, mitigates the inherent challenge to epitope shielding by glycosylation. The nanopatterning method allows for site specific conjugation to any protein. We have shown this by incorporating unnatural amino acids for direct bioconjugation to shielding molecules and by peptide insertion to allow for enzyme mediated conjugation (in the case of the spycatcher-spytag approach). This method could potentially be useful for various

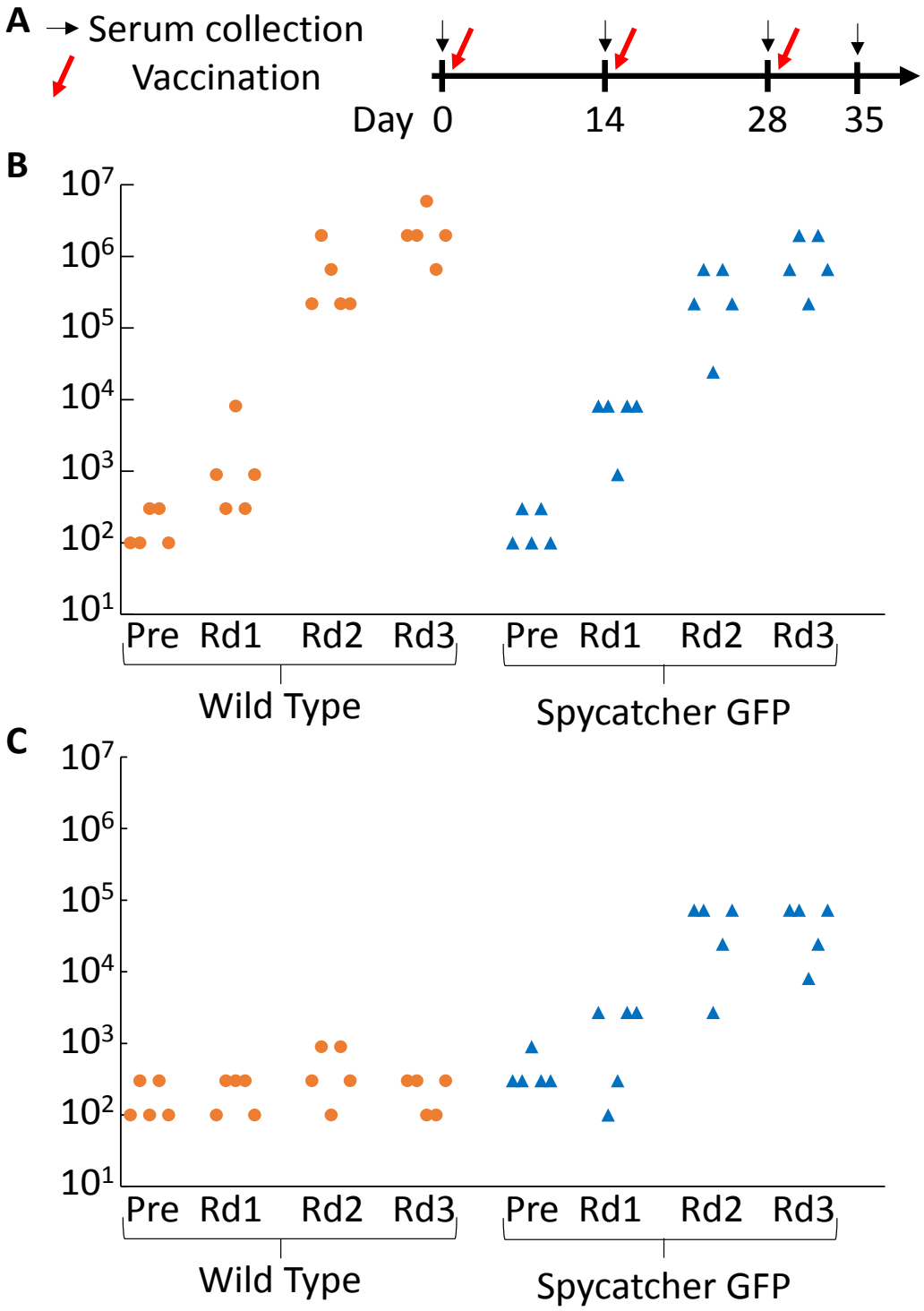

Figure 29. Wild Type and Spycatcher-GFP immunization results. (A) Immunization schedule. (B) Serum endpoint titers to Wild-type GFP, using wild-type GFP (orange circles), and spycatcher GFP (blue tirangles) as antigens. (C) Serum enpoint titers against spycatcher, same legend as in (B).

vaccine targets where a guided immune response would be beneficial (such as to the stalk domain of HA).

4.2 Future work

We are currently looking at nanopatterning other pathogenic proteins to direct the immune response to key epitopes (influenza HA, and Zika DIII). Additionally, we have not studied the importance of the specific molecule that is used to shield the protein epitope. This could be done first in ELISA by testing such things as branched PEGs, glycans, or dendrimers. The insertion of unnatural amino acids or peptides for conjugation has been done thus far by trial and error. Optimizing the location of mutations and the length of peptide insertions could enhance the ability to more directly and fully block epitopes of interest.

CHAPTER 5. INDUCING CELLULAR SIGNALING THROUGH MULTIVALENCY BY CONTROLLING LIGAND DISPLAY ON POLYMER AND POLYPEPTIDE SCAFFOLDS

5.1 Introduction

It has been established herein that multivalent molecules can induce and proliferate cell-signaling pathways in diverse cells[26-35]. It is clear from the literature that different scaffolds and conjugation densities of ligands on those scaffolds can drastically change the effectiveness of a multivalent molecule to induce signaling[31,32,88]. Still, because most multivalent molecules are based on polymer backbones that are randomly activated, it has been difficult to test how the parameters of ligand valency and inter-ligand spacing modulate the effectiveness of these molecules[88]. We have developed a polypeptide-based scaffold that allows for precise control of both valency and spacing to enable the study of these two parameters independently. We have used these scaffolds to test how the spacing of Ephrin B4 peptides changes signaling potential and have developed a method to test these same parameters within the Wnt signaling cascade.

Wnt signaling is vital for embryonic development, can induce stem cell signaling, and is implicated in cancer growth[89–91]. It is interesting among signaling pathways because of its use of two surface receptors. As shown in Figure 33, soluble Wnt binds to both LRP6 and Frizzled (FZD) and the induced co-clustering of the receptors induces downstream effects[92]. It has also been shown that clustering LRP6 alone can either initiate or enhance Wnt signaling[89,93,94]. Furthermore, Wnt is an inherently complex protein with several

posttranslational modifications, including 10 disulfide bonds and a lipid modification. Just recently, Janda et al. developed a synthetic Wnt molecule based on protein design strategies and natural LRP6 ligands[95]. Even with this development, the fact that LRP6 clustering plays a role in signal strength leads us to hypothesize that higher valency molecules may have therapeutic advantages. We have therefore developed a platform to test multivalent Wnt agonists that can enhance or induce Wnt signaling.

5.2 Materials and methods

5.2.1 Generation of polypeptide scaffolds

DNA encoding base scaffolds $[(SE)_{10}K]_{10}SE_{10}H_{10}$ and $[(SE)_{30}K]_{10}SE_{30}H_{10}$ were E. coli optimized and synthesized by Gensript. Shorter constructs were them assembled by deleting segments of the DNA by site-directed mutagenesis. Coding DNA was cloned into pet28b between Nde1 and XhoI. Protein scaffolds were expressed in BL21(DE3). After expression, cells were lysed by sonication, and the cell lysate was heated to 70^{o}C for 30 min and then clarified by centrifugation. Proteins were purified from clarified lysate using Ni-NTA resin via standard protocols.

5.2.2 Activating polypeptide scaffolds

Purified scaffold proteins were first activated by adding an NHS-malemide crosslinker, SMCC in excess to the number of lysines on the scaffold. After desalting, activated backbones were added to excess peptides with free sulfhydyl groups. Fully activated scaffolds were purified from the reaction mixture by buffer exchange through a 10 kDa MWCO spin filter.

5.2.3 Stem cell signalling tests

Stem cell signalling tests were performed by our collaborators at UC Berkeley. In short, adult neural stems cells were grown under standard conditions. Polypeptide scaffolds were activated with peptides from Ephrin-B4 and conjugated multivalent molecules were added to cell culture media. Cells were then stained for nuclei (DAPI) and for βIII-tubulin as a differentiated neural cell marker, and imaged using confocal microscopy. The percentage of cells positively staining for βIII-tubulin was reported.

5.2.4 Antibody and Fab expression and purification

The variable regions of LRP6- and Fzd-binding antibodies were cloned into the TGEX vector series for expression as full length antibodies and Fab fragments. Proteins were expressed in HEL293F cells and purified by affinity chromatography on protein A or protein L resins.

5.2.5 Wnt responsive luciferase reporter assay

HEK293T cells were stably transfected with a 7TFP reporter plasmid that expresses luciferase under the control of β-catenin. 7TFP was a gift from Roel Nusse (Addgene plasmid # 24308)[96] . Cells were transiently transfected with Wnt1 or Wnt3a and after 24 hours, were replated at 50000 cells/well of a 96-well plate. At this point, antibodies or multivalent conjugates were added, and after 16 hrs, cells were lysed and the luciferase activity was measured.

5.3 Results

5.3.1 Expression and characterization of protein-based multivalent scaffolds

Polypeptide-based scaffolds were expressed in E coli and purified over Ni-NTA. The high solubility of the scaffolds allows for a heated pre-treatment of cellular lysates to clear host cell proteins. The expression yield was low, from 0.2-5 mg/L culture, necessitating the pretreatment step to enhance protein capture on the Ni-NTA resin. Figure 30 shows three purified scaffolds that have the same inter-reactive residue spacing and differ only in valency. Each of the scaffolds were tested in circular dichroism to confirm a largely random coil structure. Regardless of scaffold length, all of these protein-based scaffolds exist in primarily random coil structures, making them behave similar to a polymer scaffold in solution.

5.3.1 Activation with Ephrin-B4 peptide and stem cell differentiation.

Scaffolds were then activated with NHS-malemide (SMCC) followed by a 2 kDa peptide from Ephrin B4. The percentage of cells that differentiated into full neurons was tracked by the expression of βIII-tubulin. Interestingly, the scaffold with the longer spacing between ligands (Figure 32) showed higher cell signaling than the shorter inter-ligand spacing. We hypothesize this is because the longer spacing better matches the distance spanned between clustered Eph receptors.

5.3.2 Wnt Signaling assay

We have also developed a method to test signaling by both Wnt1 and Wnt3a. HEK293T cells have been stably transfected with a reporter plasmid carrying a luciferase gene downstream a β-catenin control element. Mammalian expression plasmids carrying

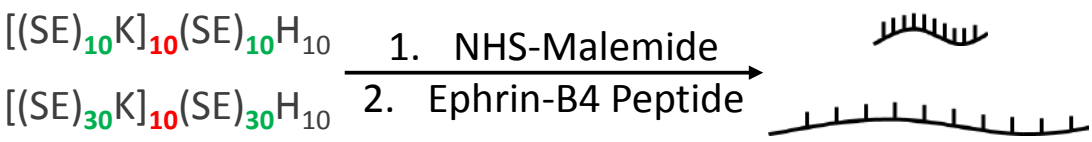

Figure 30. Polypeptide scaffolds for multivalent display. Polypeptide scaffolds are built of repeated blocks of SE repeats and a K residue. Shown are two such scaffolds. After reacting with a crosslinker, NHS-Malemide, the scaffolds are reactive to thiols and can be functionalized with protein or peptide ligands. In this depiction, the two scaffolds have been activated with an Eprin-B4 peptide, resulting in multivalent molecules that differ only in the spacing of the peptide ligands.

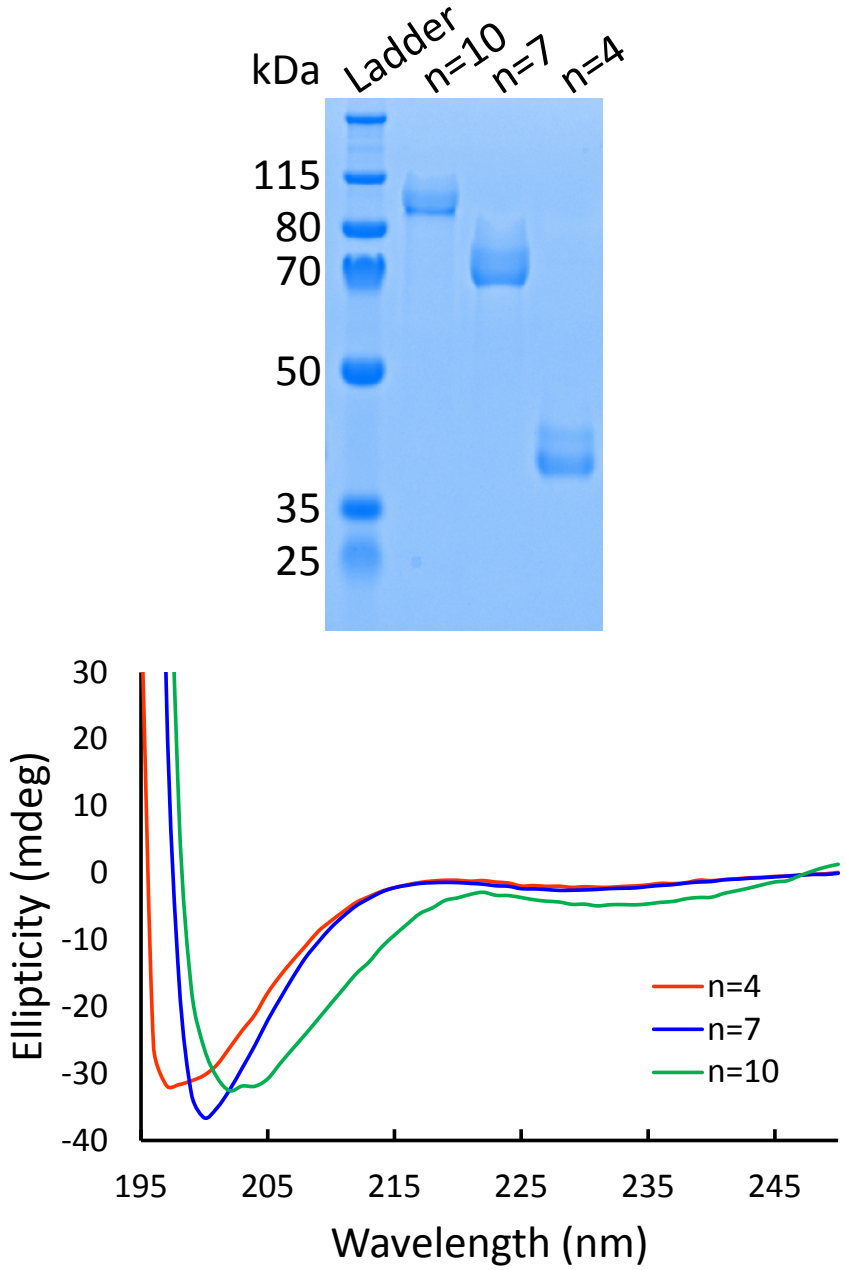

Figure 31. Expression and characterization of polypeptide scaffolds. (A) Purified $[(SE)_{30}K]_nSE_{30}H_{10}$ proteins were run on SDS-PAGE after purification. By changing the valency, n, the size of the scaffold changes while keeping the linear spacing between linkable residues the same. (B) Each of the three scaffolds purified was analyzed by circular dichroism to verify the secondary structure. The large dip in the CD spectra at ~197nm is indicative of random coils.

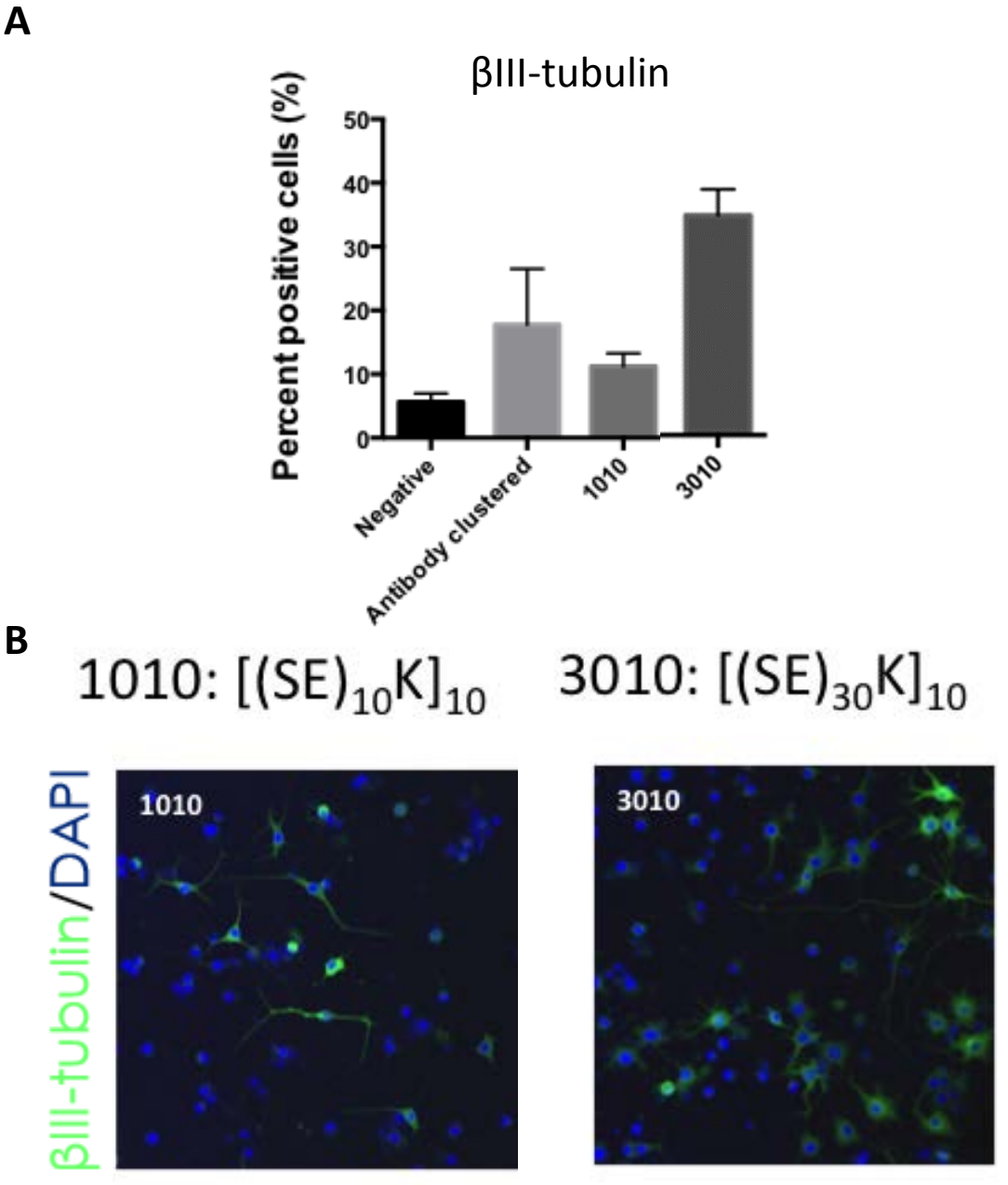

Figure 32. Induced Ephrin-B4 signaling using polypeptide scaffolds. (A) Percent of cells staining positively for βIII-tubulin, a neural cell marker in response to treatment with Ephrin signaling molecules. Cells treated with antibody or [(SE)10K]10(SE)10H10 are not as effective as cells treated with [(SE)30K]10(SE)30H10. (B) Representative confocal micrographs of cells activated with multivalent Ephrin-B4 peptide.

genes for either Wnt1 or Wnt3a are then transiently transfected into cells and after 24 hoursthe cells are plated in the final assay and incubated for 16 hrs. A time course experiment (Figure 34) has shown us that 16 hours post-plating the luciferase activity is well within the dynamic range of the assay will allow us to see both up and down regulation of Wnt signaling.

5.3.1 Antibody mediated signal inhibition

We first tested whether the expressed Fzd binding antibody would compete for Wnt binding and signaling on HEK293T cells. Indeed, for both isoforms of Wnt, anti-Fzd antibody blocks Wnt signaling, where as a control antibody has no effect (Figure 35). This result confirms that we have antibodies that bind to Fzd and can be used in multivalent constructs.

5.4 Discussion

We have shown that by using a polypeptide scaffold we can directly control the ligand spacing and valency in a multivalent conjugate. These scaffolds can be useful tools in studying diverse signaling pathways, and have potential use as therapeutic molecules. The design of the SE backbone provides both flexibility and solubility allowing even hydrophobic ligands to be attached to the scaffolds. Further, having the scaffolds designed with only the reactive residue coded genetically can allow for one to quickly screen valency and ligand spacing at will for any ligand/signaling pathway of choice. We have also developed an assay to test Wnt signaling modulation in response to multivalent molecules. While the polypeptide scaffolds can give precise ligand placement, the presence of two

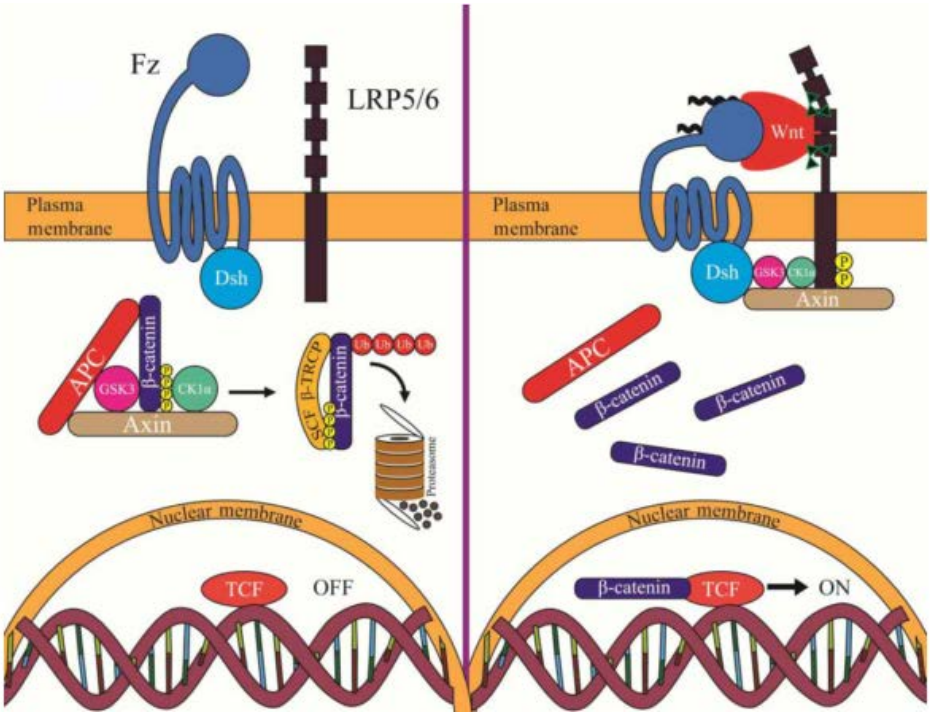

Figure 33. Mechanism of Wnt signaling[92]. Wnt binds the extracellular domains of Fzd and LRP5/6. Creation of a signalsome frees β-catenin to enter into the nucleus and turn on downstream genes. Reprinted from Saito-diaz, 2013 with permission.

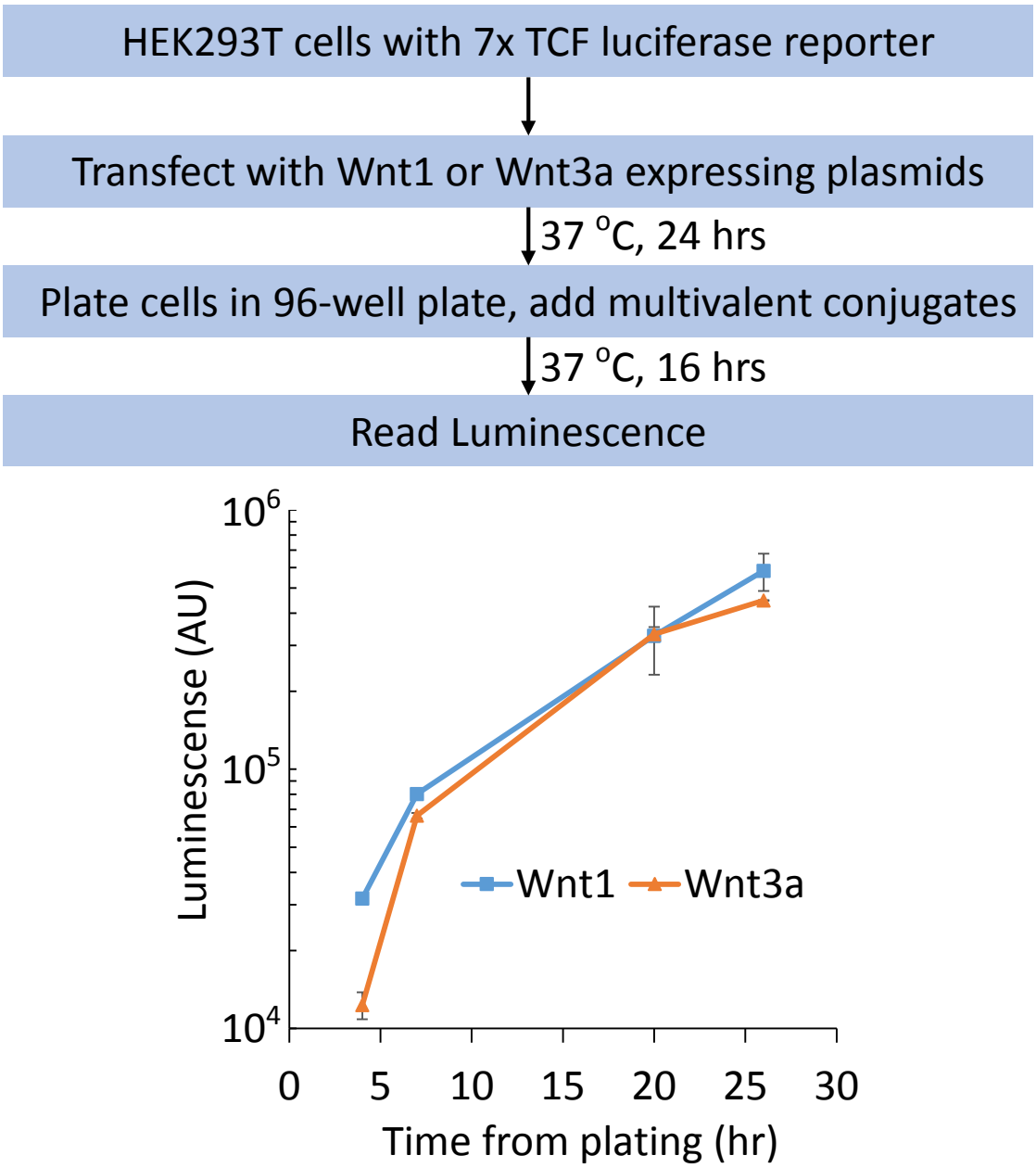

Figure 34. Wnt signaling assay development. Schematic of Wnt signaling assay including a time course experiment verify that after cell lysis, we are detecting luciferase activity in a dynamic ranges that will allow for both upregulation and down regulation to be seen.

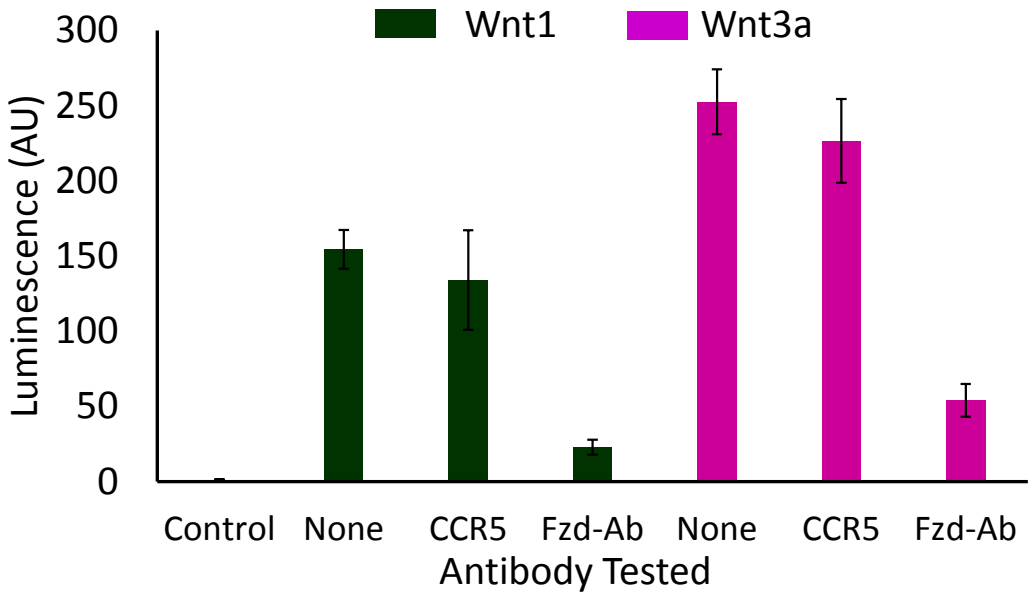

Figure 35. Anti-Fzd Ab inhibits Wnt signaling. Soluble monoclonal antibodies were added to cells after transfection with wnt expressing plasmids. Anti-CCR5 showed no inhibition of signaling, while anti-Fzd blocked Wnt signaling from both Wnt1 and Wnt3a.

receptors in Wnt signaling may necessitate more sophisticated scaffolds to probe the importance of both receptors and the make-up of potent signalosomes.

5.1 Future work

Going forward, we will be expressing LRP6-binding antibodies and Fabs and using them in conjunction with anti-FZD antibodies to generate multivalent activators of Wnt signaling. We are also working to generate a larger library of polypeptide scaffolds that could be used off the shelf to test the optimal valency and ligand spacing of multivalent molecules.

CHAPTER 6. CONCLUSION

We have applied multivalency to vaccine design and stem cell signaling. By controlling the presentation of antigens, both on scaffolds and by nanopatterning, we have been able to alter the cellular responses to the proteins. We have seen, firstly, that reversing the orientation of HA on the surface of a VLP-based vaccine can redirect the immune response toward the conserved stalk domain of HA. These stalk-reactive antibodies have the potential to be broadly active against multiple strains of influenza. We are also probing the importance of site Ø in generating broadly neutralizing antibodies against RSV. Additionally, we have developed ways to nanopattern protein antigens with the potential to redirect the immune response toward desirable epitopes. Lastly, we have developed scaffolds that can present well-defined multivalent ligands to induce cell signaling pathways including the Eph-ephrin and Wnt signaling pathways. The ability to control the multivalent and nanoscale presentation of proteins to cells in a precise manner has thus been shown to give us a tool to control and direct cellular functions.

CHAPTER 7. FUTURE DIRECTIONS

I would like to have the principles developed in my thesis work applied to more systems. I have developed methods to alter the orientation of antigens on a vaccine particle as well as to nanopattern antigens. Both approaches can potentially lead to redirecting the immune response to more efficacious epitopes on pathogenic proteins. The future work in this area is myriad, but our lab is already pursuing orientation and nanopatterning strategies with the Zika envelope DIII protein, malarial pfRH5 and MSP1 and Dengue envelope proteins. Additionally, we are looking at alternative methods for nanopatterning HA and controlling the orientation of HA. In these developments, we are looking at different scaffold architectures for orientation that can better present a desired epitope. We have realized that there are many ways to nanopattern protein antigens and that they are not all equal. Therefore, there will need to be much future work done to study and understand how to best nanopattern proteins to get good blockage of certain epitopes while redirecting the response to other regions of the protein.

The polypeptide scaffolds have the potential to become “off the shelf” scaffolds. Firstly, the library size needs to be expanded to more fully span possible valencies and inter-ligand spacings. Then it would nice to have scaffolds developed that can bind to more than one ligand, and that allow for testing different ratios and spacings of those. When the library of scaffolds increased in size and available complexity, I am confident that these scaffolds will provide a powerful way to study diverse signaling pathways, better understand receptor clustering and signal transduction, and even create designer inhibitors or multivalent binders to specific pathogens or pathways.

REFERENCES

(1) Mammen, M.; Choi, S.-K.; Whitesides, G. M. *Angew. Chem. Int. Ed. Engl.* **1998**, *30*, 2754–2794.

(2) Joshi, A.; Kate, S.; Poon, V.; Mondal, D.; Boggara, M. B.; Saraph, A.; Martin, J. T.; Mcalpine, R.; Day, R.; Garcia, A. E.; Mogridge, J.; Kane, R. S. *Biomacromolecules* **2011**, *12*, 791–796.

(3) Rai, P.; Padala, C.; Poon, V.; Saraph, A.; Basha, S.; Kate, S.; Tao, K.; Mogridge, J.; Kane, R. S. *Nat. Biotechnol.* **2006**, *24*, 582–586.

(4) CDC. Images of Influenza Viruses http://www.cdc.gov/flu/images.htm.

(5) Sauter, N. K.; Bednarski, M. D.; Wurzburg, B. a; Hanson, J. E.; Whitesides, G. M.; Skehel, J. J.; Wiley, D. C. *Biochemistry* **1989**, *28*, 8388–8396.

(6) Wu, W.; Air, G. M. *Virology* **2004**, *325*, 340–350.

(7) Mammen, M.; Dahmann, G.; Whitesides, G. M. *J. Med. Chem* **1995**, *38*, 4179–4190.

(8) Lees, W. J.; Spaltenstein, A.; Kingery-wood, J. E.; Whitesides, G. M. **1994**, 3419–3433.

(9) Pierce, S. K. *Nat. Rev. Immunol.* **2002**, *2*, 96–105.

(10) Liu, S.; Maheshwari, R.; Kiick, K. L. *Macromolecules* **2009**, *42*, 3–13.

(11) Vance, D.; Shah, M.; Joshi, A.; Kane, R. S. *Biotechnol. Bioeng.* **2008**, *101*, 429–434.

(12) Joshi, A.; Kate, S.; Poon, V.; Mondal, D.; Boggara, M.; Saraph, A.; Martin, J.; Ashton, R.; Mogridge, J.; Schaffer, D. V; Kane, R. S. **2008**, 56546.

(13) Varner, C. T.; Rosen, T.; Martin, J. T.; Kane, R. S. *Biomacromolecules* **2015**, *16*, 43–55.

(14) Fasting, C.; Schalley, C. a; Weber, M.; Seitz, O.; Hecht, S.; Koksch, B.; Dernedde, J.; Graf, C.; Knapp, E.-W.; Haag, R. *Angew. Chem. Int. Ed. Engl.* **2012**, *51*, 10472–10498.

(15) Yildiz, I.; Shukla, S.; Steinmetz, N. F. *Curr. Opin. Biotechnol.* **2011**, *22*, 901–908.

(16) Salata, O. V. *J. Nanobiotechnology* **2004**, *2*.

(17) Wang, M.; Thanou, M. *Pharmacol. Res.* **2010**, *62*, 90–99.

(18) De, M.; Ghosh, P. S.; Rotello, V. M. *Adv. Mater.* **2008**, *20*, 4225–4241.

(19) Rhee, J.-K.; Baksh, M.; Nycholat, C.; Paulson, J. C.; Kitagishi, H.; Finn, M. G. *Biomacromolecules* **2012**, *13*, 2333–2338.

(20) Kwon, C.; Kang, Y. J.; Jeon, S.; Jung, S.; Hong, S. Y.; Kang, S. *Macromol. Biosci.* **2012**, *12*, 1452–1458.

(21) Zhao, W.; Cui, C. H.; Bose, S.; Guo, D.; Shen, C.; Wong, W. P.; Halvorsen, K.; Farokhzad, O. C.; Teo, G. S. L.; Phillips, J. a; Dorfman, D. M.; Karnik, R.; Karp, J. M. *Proc. Natl. Acad. Sci. U. S. A.* **2012**, *109*, 19626–19631.

(22) Kiessling, L. L.; Gestwicki, J. E.; Strong, L. E. *Curr. Opin. Chem. Biol.* **2000**, *4*, 696–703.

(23) Kiessling, L. L.; Gestwicki, J. E.; Strong, L. E. *Angew Chem Int Ed.* **2006**, *45*, 2348–2368.

(24) Vorup-Jensen, T. *Adv. Drug Deliv. Rev.* **2012**, *64*, 1759–1781.

(25) Sil, D.; Lee, J. B.; Luo, D.; Holowka, D.; Baird, B. *ACS Chem. Biol.* **2007**, *2*, 674–684.

(26) Handlogten, M. W.; Kiziltepe, T.; Alves, N. J.; Bilgicer, B. *ACS Chem. Biol.* **2012**, *7*, 1796–1801.

(27) Handlogten, M. W.; Kiziltepe, T.; Bilgicer, B. *Biochem. J.* **2013**, *449*, 91–99.

(28) Huang, Y.-F.; Liu, H.; Xiong, X.; Chen, Y.; Tan, W. *J. Am. Chem. Soc.* **2009**, *131*, 17328–17334.

(29) Bennett, N. R.; Zwick, D. B.; Courtney, A. H.; Kiessling, L. L. *ACS Chem. Biol.* **2015**, *10*, 1817–1824.

(30) Courtney, A. H.; Puffer, E. B.; Pontrello, J. K.; Yang, Z.-Q.; Kiessling, L. L. *Proc. Natl. Acad. Sci. U. S. A.* **2009**, *106*, 2500–2505.

(31) Conway, A.; Vazin, T.; Spelke, D. P.; Rode, N. a; Healy, K. E.; Kane, R. S.; Schaffer, D. V. *Nat. Nanotechnol.* **2013**, *8*, 831–838.

(32) Vazin, T.; Ashton, R. S.; Conway, A.; Rode, N. a; Lee, S. M.; Bravo, V.; Healy, K. E.; Kane, R. S.; Schaffer, D. V. *Biomaterials* **2014**, *35*, 941–948.

(33) Han, S.; Lee, M.; Lim, Y. *Biomacromolecules* **2013**, *14*, 1594–1599.

(34) Lee, L. A.; Muhammad, S. M.; Nguyen, Q. L.; Sitasuwan, P.; Horvath, G.; Wang, Q. *Mol. Pharm.* **2012**, *9*, 2121–2125.

(35) Webber, M.; Tongers, J.; Newcomb, C. J.; Marquardt, K.; Bauersachs, J.; Losordo, D. W.; Stupp, S. I.; Webber, M. J. *Proc. Natl. Acad. Sci.* **2012**, *109*, 9220–9220.

(36) Krammer, F.; Palese, P. *Nat. Rev. Drug Discov.* **2015**, *14*, 167–182.

(37) Moody, M. A. et al. *PLoS One* **2011**, *6*, e25797.

(38) Wrammert, J. et al. *Nature* **2008**, *453*, 667–671.

(39) Margine, L. et al. *J. Virol.* **2013**, *87*, 4728–4737.

(40) Krammer, F.; Palese, P. *Nat. Immunol.* **2014**, *13*, 3–5.

(41) Andrews, S. F. et al. *Sci. Transl. Med.* **2015**, *7*, 316ra192.

(42) Ekiert, D. C. et al. *Science (80-.).* **2009**, *324*, 246–251.

(43) Ekiert, D. C.; Wilson, I. A. *Curr. Opin. Virol.* **2012**, *2*, 134–141.

(44) Tan, G. S. et al. *J. Virol.* **2012**, *86*, 6179–6188.

(45) Wang, T. T. et al. *PLoS Pathog.* **2010**, *6*, e1000796.

(46) Krammer, F., Pica, N., Hai, R., Margine, I. & Palese, P. *J. Virol.* **2013**, *87*, 6542–6550.

(47) Ekiert, D. C. et al. *Science (80-.).* **2011**, *333*, 843–850.

(48) Throsby, M. et al. *PLoS One* **2008**, *3*, e3942.

(49) Margine, L. et al. *J. Virol.* **2013**, *87*, 10435–10446.

(50) Kaneyiko, M. et al. *Nature* **2013**, *499*, 102–106.

(51) Implagliazzo, A. et al. *Science (80-.).* **2015**, *349*, 1301–1306.

(52) Yassine, H. M. et al. *Nat. Med.* **2015**, *21*, 1065–1070.

(53) Bommakanti, G. et al. *J. Virol.* **2012**, *86*, 13434–13444.

(54) Lu, Y., Welsh, J.P. & Swartz, J. R. *Proc. Natl. Acad. Sci.* **2014**, *111*, 125–130.

(55) Mallajosyula, V. V. a.; Citron, M.; Ferrara, F.; Lu, X.; Callahan, C.; Heidecker, G. J.; Sarma, S. P.; Flynn, J. a.; Temperton, N. J.; Liang, X.; Varadarajan, R. *Proc. Natl. Acad. Sci.* **2014**.

(56) Steel, J. et al. *Macromol Biosci* **2010**, *1*.

(57) Graves, P.N., Schulman, J.L., Young, J.F. & Palese, P. *Virology* **1983**, *126*, 106–116.

(58) Sagawa, H., Ohshima, A., Kato, I., Okuno, Y. & Isegawa, Y. *J. Gen. Virol.* **1996**, *77*, 1483–1487.

(59) Jennings, G. T.; Bachmann, M. F. *Biol. Chem.* **2008**, *389*, 521–536.

(60) Schneemann, A.; Speir, J. a; Tan, G. S.; Khayat, R.; Ekiert, D. C.; Matsuoka, Y.; Wilson, I. a. *J. Virol.* **2012**, *86*, 11686–11697.

(61) Patel, K. G.; Swartz, J. R. *Bioconjug. Chem.* **2011**, *22*, 376–387.

(62) Peabody, D. S.; Manifold-Wheeler, B.; Medford, A.; Jordan, S. K.; do Carmo Caldeira, J.; Chackerian, B. *J. Mol. Biol.* **2008**, *380*, 252–263.

(63) Margine, I.; Palese, P.; Krammer, F. *J. Vis. Exp.* **2013**, *81*, 51112.

(64) Golmohammadi, R.; Valegård, K.; Fridborg, K.; Liljas, L. *J. Mol. Biol.* **1993**, *234*, 620–639.

(65) Schmidt, T. G. M.; Koepke, J.; Frank, R.; Skerra, A. *J. Mol. Biol.* **1996**, *255*, 753–766.

(66) Ruigrok, R. In *Textbook of Influenza*; KG Nicholson, RG Webster, A. H., Ed.; Blackwell Science, 1998; pp. 29–42.

(67) Karl D. Brune, Darren B. Leneghan, Iona J. Brian, Andrew S. Ishizuka, Martin F. Bachmann, Simon J. Draper, Sumi Biswas, M. H. *Sci. Rep.* **2016**, *6*, 19234.

(68) Bundy, B. C.; Franciszkowicz, M. J.; Swartz, J. R. *Biotechnol. Bioeng.* **2008**, *100*, 28–37.

(69) Jegerlehner, A.; Zabel, F.; Langer, A.; Dietmeier, K.; Jennings, G. T.; Saudan, P.; Bachmann, M. F. *PLoS One* **2013**, *8*, e78947.

(70) Warfield, K. L.; Swenson, D. L.; Olinger, G. G.; Kalina, W. V; Aman, M. J.; Bavari, S. *J. Infect. Dis.* **2007**, *196 Suppl* , S430–S437.

(71) Wu, P.; Harter, T. V. *Expert Rev Anti Infect* **2011**, *9*, 731–745.

(72) Neuzil, K. M. *Clin Vaccine Immunol* **2016**, *23*, 186–188.

(73) Dudas, R. A.; Karron, R. A. *Clin Microbiol Rev* **1998**, *11*, 430–439.

(74) Jia Meng; Stobart, C. C.; Hotard, A. L.; Moore, M. L. *PLoS Pathog.* **2014**, *10*, E10004016.

(75) McLellan, J. S.; Ray, W. C.; Peeples, M. E. *Curr Top Microbiol Immunol* **2013**, *372*, 83–104.

(76) Ngwuta, J. O.; Chen, M.; Modjarrad, K.; Joyce, M. G.; Kanekiyo, M.; Kumar, A.; Yassine, H. M.; Moin, S. M.; Killikelly, A. M.; Chuang, G.; Druz, A.; Georgiev, I. S.; Rundlet, E. J.; Sastry, M.; Stewart-Jones, G. B. E.; Yang, Y.; Zhang, B.; Nason, M. C.; Capella, C.; Peeples, M. E.; Ledgerwood, J. E.; McLellan, J. S.; Kwong, P. D.; Graham, B. S. *Sci. Transl. Med.* **2015**, *7*, 309ra162.

(77) McLellan JS, Chen M, Joyce MG, Sastry M, Stewart-Jones GB, Yang Y, Zhang B, Chen L, Srivatsan S, Zheng A, Zhou T, Graepel KW, Kumar A, Moin S, Boyington JC, Chuang GY, Soto C, Baxa U, Bakker AQ, Spits H, Beaumont T, Zheng Z, Xia N, Ko SY, Todd JP, Rao S, K. P. *Science (80-.).* **2013**, *342*, 592–598.

(78) McLellan JS, Chen M, Leung S, Graepel KW, Du X, Yang Y, Zhou T, Baxa U, Yasuda E, Beaumont T, Kumar A, Modjarrad K, Zheng Z, Zhao M, Xia N, Kwong PD, G. B. *Science (80-.).* **2013**.

(79) Krarup A; D, T.; P, F.-H.; Al., E. *Nat. Commun.* **2015**, *6*, 8143.

(80) Reitter JN, Means RE, D. R. *Nat. Med.* **1998**, *4*, 679–684.

(81) Wei X, Decker JM, Wang S, Hui H, Kappes JC, et al. *Nature* **2003**, *422*, 307–312.

(82) Eggink D, G. P.; P, P. *J. Virol.* **2014**, *88*, 699–704.

(83) Lanying Du, Wanbo Tai, Yang Yang, Guangyu Zhao, Qing Zhu, Shihui Sun, Chang Liu, Xinrong Tao, Chien-Te K. Tseng, Stanley Perlman, Shibo Jiang, Y. Z. & F. L. *Nat. Commun.* **2016**, *7*.

(84) Jardine J, Julien JP, Menis S, Ota T, Kalyuzhniy O, et al. *Science (80-.).* **2013**, *340*, 711–716.

(85) Horiya S, MacPherson IS, K. I. *Nat. Chem. Biol.* **2014**, *10*, 990–999.

(86) Numata, J.; Juneja, A.; Diestler, D. J.; Knapp, E.-W. *J. Phys. Chem. B* **2012**, *116*, 2595–2604.

(87) Amiram, M.; Haimovich, A. D.; Fan, C.; Wang, Y.-S.; Ntai, I.; Moonan, D. W.; Ma, N. J.; Rovner, A. J.; Hoon, S.; Kelleher, N. L.; Goodman, A. L.; Jewett, M. C.; Söll, D.; Rinehart, J.; Isaacs, F. J. *Nat. Biotechnol.* **2015**, *33*, 1272–1278.

(88) Patke, S.; Boggara, M.; Maheshwari, R.; Srivastava, S. K.; Arha, M.; Douaisi, M.; Martin, J. T.; Harvey, I. B.; Brier, M.; Rosen, T.; Mogridge, J.; Kane, R. S. *Angew. Chem. Int. Ed. Engl.* **2014**, *53*, 1–5.

(89) Cong, F.; Schweizer, L.; Varmus, H. *Development* **2004**, *131*, 5103–5115.

(90) Holland, J. D.; Klaus, A.; Garratt, A. N.; Birchmeier, W. *Curr. Opin. Cell Biol.* **2013**, *25*, 254–264.

(91) Anastas, J. N.; Moon, R. T. *Nat. Rev. Cancer* **2013**, *13*, 11–26.

(92) Saito-diaz, K.; Chen, T. W.; Wang, X.; Thorne, C. a; Wallace, H. a; Page-mccaw, A.; Lee, E. *Growth Factors* **2013**, *31*, 1–31.

(93) Bugaj, L. J.; Choksi, A. T.; Mesuda, C. K.; Kane, R. S.; Schaffer, D. V. *Nat. Methods* **2013**, *10*, 249–252.

(94) Binnerts, M. E.; Kim, K.-A.; Bright, J. M.; Patel, S. M.; Tran, K.; Zhou, M.; Leung, J. M.; Liu, Y.; Lomas, W. E.; Dixon, M.; Hazell, S. a; Wagle, M.; Nie, W.-S.; Tomasevic, N.; Williams, J.; Zhan, X.; Levy, M. D.; Funk, W. D.; Abo, A. *Proc. Natl. Acad. Sci. U. S. A.* **2007**, *104*, 14700–14705.

(95) Claudia Y. Janda, Luke T. Dang, Changjiang You, Junlei Chang, Wim de Lau, Zhendong A. Zhong, Kelley S. Yan, Owen Marecic, Dirk Siepe, Xingnan Li, James D. Moody, Bart O. Williams, Hans Clevers, Jacob Piehler, David Baker, C. J. K. & K. C. G. *Nature* **2017**, *advance on*, doi:10.1038/nature22306.

(96) C, F.; R, N. *PLoS One* **2010**, *5*, 39370.